

PRODUCTION OF DEUTERONS AND PIONS IN A TRANSPORT MODEL OF ENERGETIC HEAVY-ION REACTIONS

P. DANIELEWICZ and G.F. BERTSCH

*National Superconducting Cyclotron Laboratory and Department of Physics and Astronomy,
Michigan State University, East Lansing, MI 48824, USA*

Received 8 April 1991
(Revised 21 May 1991)

Abstract: Green functions are used to derive transport equations with bound-state production and absorption. The equations are valid in the quasiparticle limit and are used to describe deuteron production in heavy-ion induced reactions. The deuterons are produced in three-nucleon collisions in a process that is inverse to deuteron breakup. We also derive rate equations for pion production by resonance formation and decay. Our equations satisfy detailed balance even in the case of wide resonances, unlike previous formulations. The relation widely employed in the cascade and Boltzmann equation models produces an equilibrium with too many pions. We have solved the equations numerically, finding for a number of cases fair agreement with experimental data. The predicted entropy produced in central Nb + Nb collisions at 650 MeV/nucleon exceeds by half a unit the entropy deduced from data. The predicted pion yields in the cascade limit are much closer to the data measured in central Ar + KCl collisions than was found in earlier treatments.

1. Introduction

A full description of heavy-ion-induced reactions requires other degrees of freedom besides the nucleon single-particle variables. A distinct feature of high-energy reactions is the large number of composites, particularly deuterons, emitted into wide angles¹⁾. The theory of deuteron production by heavy ions was at first rather crude. Models were based on various assumptions including: chemical equilibrium²⁻⁵⁾, coalescence in momentum space⁶⁻⁸⁾, and coalescence in phase space^{9,10)}. The first theory based on dynamics was proposed by Remler¹¹⁾, and was applied in refs. ^{12,13)}. Dynamic models relying on nucleon degrees of freedom and independent nucleon-nucleon collisions¹⁴⁻¹⁷⁾ have been quite successful in describing single-particle features such as production of protons. Although the quasiparticle assumption inherent in the models may not be well satisfied in reactions, see e.g. ref. ¹⁸⁾, these models are appealing because they incorporate a range of dynamic effects and are computationally tractable. In this paper we examine the extension of the models beyond the approximation that the equations can be truncated with two-particle collisions and only nucleon degrees of freedom. We

shall incorporate deuteron production within the present framework by incorporating three-body collision terms.

The pion degrees of freedom are also significant for heavy-ion reactions in the energy domain of hundreds of MeV per nucleon. The production of pions received particular attention^{19–22)} after data were compared with the predictions of thermodynamic^{2,23)} and cascade models^{14,24–27)}. In the cascade it was assumed that pions can be treated by adding the delta degree of freedom to the nucleons. The respective procedure is routinely applied in dynamic models^{16,17,28–34)}.

An important claim in the literature has been that the simple cascade predicts too many pions, and indeed, that one can obtain information about the nuclear equation of state from pion yields. The discrepancy between cascade and experiment has been directly used to extract the equation of state^{20–22,35–37)}. However, our analysis produces a different formula for the cross sections than what is commonly assumed in dynamic models. We shall see that pion yields from the corrected rate equations are much closer to the data for the simple cascade, and that the sensitivity to the potential field is weak.

In sect. 2 we derive a transport equation for deuterons including deuteron production and absorption terms. We further study limits in momentum space for the existence of a discrete state in deuteron channel. In sect. 3 we discuss the deuteron production and absorption rates and the realization of thermodynamic equilibrium. The formation of deuterons becomes similar to that in the approach by Remler *et al.* [refs.^{12,13)}]*, when an impulse approximation is used for the matrix element in the rates. We use the data for deuteron breakup to parametrize the square of matrix element.

In sect. 4 we discuss the production of pions through the formation and decay of baryon resonances. We show that the detailed balance relation used in past calculations of pion production is not valid when the unstable particles have broad widths. In general, the reabsorption cross section of broad resonances is underestimated in previous treatments. This leads, in consequence, to an equilibrium with too many pions. We derive another relation for determining the resonance reabsorption cross section, expressed in eqs. (4.14)–(4.16). In sect. 5 we discuss the parametrization of single-particle energies in the calculations.

The numerical method of solving the set of transport equations is discussed in the appendix. Our method differs from previous treatments employing pseudo-particles in several respects. Besides the introduction of three-body collisions we use a different method for treating the effects of the Pauli principle in binary collisions. The results of the calculations are compared in sect. 6 with a variety of data on particle production^{1,38)}. We also examine the production of entropy, which in our treatment is calculated from the quasiparticle distribution functions. This contrasts with the thermodynamic treatments of deuteron production, which assume

* We note that the method of refs.^{12,13)} does not produce correct thermodynamic equilibrium in the limit of long interaction times.

a direct connection between deuteron yields and entropy. Finally, we study the sensitivity of the produced entropy, d/p ratio, and pion multiplicity to the nuclear equation of state. We conclude with a discussion in sect. 7.

2. Deuteron transport equation

We shall describe deuterons with the help of a two-particle Green function that is defined on a contour in time^{18,39,40)}

$$iG_2(x_1, x_2, t, x'_1, x'_2, t') = \langle T\{\psi(x_1, t)\psi(x_2, t)\psi^\dagger(x'_2, t')\psi^\dagger(x'_1, t')\} \rangle. \quad (2.1)$$

Here x labels the position as well as the particle spin and isospin states, $x \equiv (\mathbf{r}, a, \alpha)$. The deuteron occupation will be obtained from the function

$$iG_2^<(x_1, x_2, t, x'_1, x'_2, t') = \langle \psi^\dagger(x'_2, t')\psi^\dagger(x'_1, t')\psi(x_1, t)\psi(x_2, t) \rangle, \quad (2.2)$$

which is a particular case of (2.1).

The function G_2 satisfies an equation which follows from diagrammatic expansion^{41,18)} of the expectation value in (2.1),

$$G_2 = \mathcal{G} + \frac{1}{4}\mathcal{G}vG_2. \quad (2.3)$$

Here v is an antisymmetrized potential, and the operator product involves a summation over indices, integration over spatial variables, and integration over a contour in time. The function \mathcal{G} is an irreducible part of G_2 which does not contain two one-particle lines connected by the potential. We have

$$\mathcal{G} = \mathcal{G}^D + \mathcal{G}^C, \quad (2.4)$$

where \mathcal{G}^D in (2.4) is a product of one-particle Green function,

$$\begin{aligned} \mathcal{G}^D(x_1, x_2, t, x'_1, x'_2, t') \\ = i(G(x_1, t, x'_1, t')G(x_2, t, x'_2, t') - G(x_1, t, x'_2, t')G(x'_1, t, x_2, t')), \end{aligned} \quad (2.5)$$

with

$$iG(x, t, x', t') = \langle T\{\psi(x, t)\psi^\dagger(x', t')\} \rangle. \quad (2.6)$$

The function \mathcal{G}^C is an irreducible part with the lines connected in some way. The lowest-order contribution to \mathcal{G}^C is shown in fig. 1.

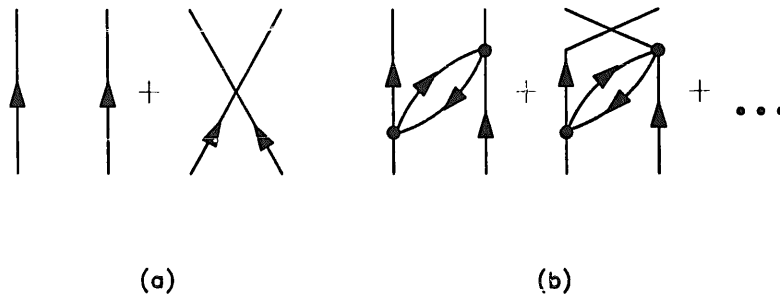


Fig. 1. Irreducible part of the two-particle Green function \mathcal{G} : (a) \mathcal{G}^D and (b) \mathcal{G}^C .

From (2.3) we obtain

$$G_2^\pm = \mathcal{G}^\pm + \frac{1}{4}\mathcal{G}^\pm v G_2^\pm, \quad (2.7)$$

with the time integration in operator product running now along ordinary time-axis. The retarded F^+ and advanced F^- functions are defined as

$$F^\pm(t, t') = \pm \theta(\pm(t - t'))(F^> - F^<)(t, t'), \quad (2.8)$$

with all arguments except the time variables suppressed. Functions $F^>$ correspond to expectation values with the creation operators on the right of annihilation operators. This is opposite of the order in eq. (2.2), cf. ref. ¹⁸). For the functions G_2^\pm we get

$$G_2^\pm = \mathcal{G}^\pm + \frac{1}{4}\mathcal{G}^\pm v G_2^\pm + \frac{1}{4}\mathcal{G}^\pm v G_2^\pm. \quad (2.9)$$

Combining this with (2.7) leads to

$$G_2^\pm = (1 + \frac{1}{4}G_2^\pm v)\mathcal{G}^\pm(1 + \frac{1}{4}v G_2^\pm), \quad (2.10)$$

where the operator 1 is

$$\delta(t - t')\frac{1}{2}(\delta(x_1 - x'_1)\delta(x_2 - x'_2) - \delta(x_1 - x'_2)\delta(x_2 - x'_1)).$$

A discrete state corresponds to a pole of G_2^\pm and a resonance peak in G_2^\pm when these functions are Fourier transformed in relative times. We shall develop our equations for the functions G_2 in a Wigner representation for the c.m. coordinates as well as the time variables. In this representation ^{41,18}), the functions are

$$\begin{aligned} \langle \mathbf{r} | F(\mathbf{P}, \Omega, \mathbf{R}, T) | \mathbf{r}' \rangle &= \int dT' d\mathbf{R}' e^{i(\Omega T' - \mathbf{P} \cdot \mathbf{R}')} \\ &\times F(\mathbf{R} + \frac{1}{2}\mathbf{R}' + \frac{1}{2}\mathbf{r}, \mathbf{R} + \frac{1}{2}\mathbf{R}' - \frac{1}{2}\mathbf{r}, T + \frac{1}{2}T', \mathbf{R} - \frac{1}{2}\mathbf{R}' + \frac{1}{2}\mathbf{r}', \\ &\mathbf{R} - \frac{1}{2}\mathbf{R}' - \frac{1}{2}\mathbf{r}', T - \frac{1}{2}T'). \end{aligned} \quad (2.11)$$

When a product of two such operators is Wigner transformed, the result may be expanded to yield the substitution

$$fu \rightarrow fu + \frac{1}{2}i[f, u] + \dots \quad (2.12)$$

The Poisson bracket for the transformed functions is

$$[f, u] = \frac{\partial f}{\partial \Omega} \frac{\partial u}{\partial T} - \frac{\partial f}{\partial T} \frac{\partial u}{\partial \Omega} - \frac{\partial f}{\partial \mathbf{P}} \cdot \frac{\partial u}{\partial \mathbf{R}} + \frac{\partial f}{\partial \mathbf{R}} \cdot \frac{\partial u}{\partial \mathbf{P}}. \quad (2.13)$$

Note that there is an integration over the intermediate internal variables for the Wigner-transformed functions in (2.12) and (2.13). When one of the functions has a resonance structure in energy, the averaging over an energy interval must be applied to justify dropping of higher-order terms in the expansion (2.12).

We first display the form of the functions in the vicinity of a resonance. The internal wave function in the residue of G_2^\pm , assuming weak damping, satisfies the equation

$$\int dx' \langle x | \text{Re} (G_2^+)^{-1} (P, E, R, T) | x' \rangle \langle x' | \phi (P, R, T) \rangle = 0. \quad (2.14)$$

Note that x labels now the *internal* spatial variables r and the spin and isospin indices. Further $E = E(P, R, T)$ in (2.14) is the energy of the state, and $\text{Re}(\cdot)$ denotes the hermitian part of the operator,

$$\begin{aligned} 2\langle x | \text{Re} (G_2^+)^{-1} (P, \Omega, R, T) | x' \rangle \\ = \langle x | (G_2^+)^{-1} (P, \Omega, R, T) | x' \rangle + \langle x' | (G_2^+)^{-1} (P, \Omega, R, T) | x \rangle^* \\ = \langle x | ((G_2^+)^{-1} + (G_2^-)^{-1}) (P, \Omega, R, T) | x' \rangle \\ = 2\langle x | \text{Re} (\mathcal{G}^+)^{-1} (P, \Omega, R, T) - \frac{1}{4}v | x' \rangle, \end{aligned} \quad (2.15)$$

see e.g. ref. ¹⁸). Following (2.10) we have

$$(G_2^+)^{-1} G_2^\pm = ((G_2^+)^{-1} + \frac{1}{4}v) \mathcal{G}^\pm (1 + \frac{1}{4}v G_2^\pm). \quad (2.16)$$

After Wigner transformation, the lowest-order terms yield

$$\text{Re} (G_2^+)^{-1} G_2^\pm = 0, \quad (2.17)$$

and the functions G_2^\pm in the vicinity of resonance become

$$\begin{aligned} i\langle x | G_2^< (P, \Omega, R, T) | x' \rangle = \langle x | \phi (P, R, T) \rangle \langle \phi (P, R, T) | x' \rangle \\ \times 2Z_2(P, R, T) f_2(P, R, T) 2\pi\delta(\Omega - E(P, R, T)) \end{aligned} \quad (2.18)$$

and

$$\begin{aligned} i\langle x | G_2^> (P, \Omega, R, T) | x' \rangle = \langle x | \phi (P, R, T) \rangle \langle \phi (P, R, T) | x' \rangle 2Z_2(P, R, T) \\ \times (1 + f_2(P, R, T)) 2\pi\delta(\Omega - E(P, R, T)). \end{aligned} \quad (2.19)$$

with f_2 - an occupation. We use in (2.18) and (2.19) the identity

$$G_2^> - G_2^< = G_2^+ - G_2^-, \quad (2.20)$$

and

$$\begin{aligned} Z_2^{-1}(P, R, T) = 2 \int dx dx' \langle \phi (P, R, T) | x \rangle \frac{\partial}{\partial \Omega} \langle x | \text{Re} (G_2^+)^{-1} (P, \Omega, R, T) | x' \rangle |_{\Omega=E} \\ \times \langle x' | \phi (P, R, T) \rangle. \end{aligned} \quad (2.21)$$

To obtain an equation for the variation of occupation f_2 we apply (2.12) to eq. (2.16) and retain the zeroth- and first-order terms in the expansion with respect to spatial and time derivatives. We get

$$\begin{aligned} (G_2^+)^{-1} G_2^< + \frac{1}{2}i[\text{Re} (G_2^+)^{-1}, G_2^<] \\ = (\text{Re} (G_2^+)^{-1} + \frac{1}{4}v) \mathcal{G}^+ \frac{1}{4}v(-i) \text{Im} G_2^+, \end{aligned} \quad (2.22)$$

and on subtracting from (2.22) the conjugate equation, and integrating over the internal variables, we find for f_2

$$\frac{\partial f_2}{\partial T} + \frac{\partial E}{\partial \mathbf{P}} \cdot \frac{\partial f_2}{\partial \mathbf{R}} - \frac{\partial E}{\partial \mathbf{R}} \cdot \frac{\partial f_2}{\partial \mathbf{P}} + \mathcal{D}' f_2 = \mathcal{K}^<(1 + f_2) - \mathcal{K}^> f_2. \quad (2.23)$$

The last term at the l.h.s. of (2.23) is

$$\begin{aligned} \mathcal{D}' f_2 = & \int dx dx' \left(\frac{\partial}{\partial \mathbf{R}} \langle x | \text{Re} (G_2^+)^{-1}(\mathbf{P}, E, \mathbf{R}, T) | x' \rangle \right. \\ & \times \frac{\partial}{\partial \mathbf{P}} (Z_2(\mathbf{P}, \mathbf{R}, T) f_2(\mathbf{P}, \mathbf{R}, T) \langle \phi(\mathbf{P}, \mathbf{R}, T) | x \rangle \langle x' | \phi(\mathbf{P}, \mathbf{R}, T) \rangle) \\ & - \frac{\partial}{\partial \mathbf{P}} \langle x | \text{Re} (G_2^+)^{-1}(\mathbf{P}, E, \mathbf{R}, T) | x' \rangle \\ & \left. \times \frac{\partial}{\partial \mathbf{R}} (Z_2(\mathbf{P}, \mathbf{R}, T) f_2(\mathbf{P}, \mathbf{R}, T) \langle \phi(\mathbf{P}, \mathbf{R}, T) | x \rangle \langle x' | \phi(\mathbf{P}, \mathbf{R}, T) \rangle) \right), \end{aligned} \quad (2.24)$$

and the absorption $\mathcal{K}^>$ and production $\mathcal{K}^<$ rates are

$$\begin{aligned} \mathcal{K}^\pm(\mathbf{P}, \mathbf{R}, T) = & Z_2(\mathbf{P}, \mathbf{R}, T) \frac{1}{8} i \int dx dx' \langle \phi(\mathbf{P}, \mathbf{R}, T) | x \rangle \\ & \times \langle x | v \mathcal{G}^\pm(\mathbf{P}, E, \mathbf{R}, T) v | x' \rangle \langle x' | \phi(\mathbf{P}, \mathbf{R}, T) \rangle. \end{aligned} \quad (2.25)$$

The rates may be expanded diagrammatically⁴²⁾. Upon expansion, the absorption and production can be brought into a form similar to that in the approach by Remler *et al.*¹¹⁻¹³⁾. When expanding in terms of interacting quasiparticles, an identity which holds for the one-particle functions,

$$G^\pm = G^+ \Sigma^\pm G^-, \quad (2.26)$$

is used. Eq. (2.23) represents the most general form of kinetic equation for the bound-state occupation probability.

In addition to the usual conditions for the validity of the Boltzmann equation, the derivation of (2.23) requires that $\tau_f \geq 1/(2(\langle T \rangle - E))$ is less than the time of characteristic variations in a system. The energy E is the bound-state energy and $\langle T \rangle$ is the average of the kinetic energy over the bound-state wave function. In the energy representation this becomes a condition that the resonance is well isolated. For deuterons $\tau_f \geq 4.5 \text{ fm}/c$, and the condition may only be satisfied late during the development of a heavy-ion collision.

Beyond the brief analysis that follows, we make no attempt to solve the deuteron eigenvalue problem (2.14) in a medium. Physically, in moderately dense matter a neutron-proton pair is likely to be in a composite larger than a deuteron. Indeed, the comparisons of model calculations with data are often done for d-like nucleon pairs^{9,12,13,43)}. In principle one might try to calculate the depletion of a deuteron pole in G_2 due to the dressing of deuterons with additional nucleons. With decreasing

excitation of the medium, heavy composites would need to be considered. The interior of these composites can be described as nuclear matter with nucleons only. From eq. (2.14), using \mathcal{G}^D for \mathcal{G} with G in quasiparticle approximation, we obtain the following equation for the deuteron pole

$$(E(P) - e(\tfrac{1}{2}P + p) - e(\tfrac{1}{2}P - p))\langle p | \phi \rangle - \tfrac{1}{2}(1 - f(\tfrac{1}{2}P + p) - f(\tfrac{1}{2}P - p)) \times \int \frac{d\mathbf{p}'}{(2\pi)^3} \langle p | v | p' \rangle \langle p' | \phi \rangle = 0. \quad (2.27)$$

This equation was considered previously⁴⁴⁻⁴⁶), and it accounts for the effects of antisymmetrization with nucleons in surrounding matter and of the single-particle spectrum on the two-body state. The antisymmetrization removes the particle-hole components from the wave function at zero temperature.

We solve eq. (2.27) at zero temperature in the deuteron channel, averaging over angles in the factor $(1 - f - f)$, and setting $m^* = m$. We report here the results for the separable potential⁴⁷) of Graz form including tensor interactions, but we have tried a potential without tensor coupling with very similar results. Fig. 2 shows the region in which there is a discrete pole in the two-body Green function as a function of p_F and P . The region, marked “deuteron” and “Cooper pair”, is bordered by a solid line. At low densities the state exists for all values of P , but at higher density ($\rho \geq 5 \times 10^{-3} \text{ fm}^{-3} \approx \rho^0/30$) there are two branches. The higher momentum states can be identified with deuterons separated in phase space from the nuclear matter, but perturbed by the antisymmetrization. The lower branch represents Cooper pairs

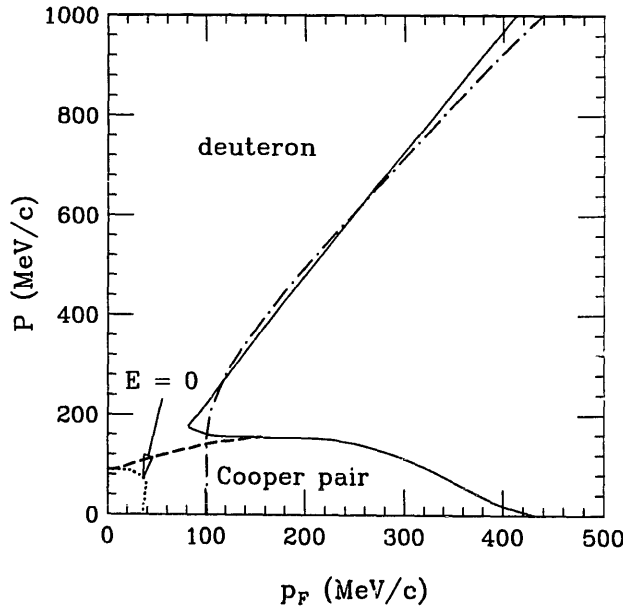


Fig. 2. The P - p_F plane, showing the region in which the neutron-proton Green function has a discrete pole. Here P is the total momentum of a pair and p_F is the Fermi momentum of nuclear medium. The region with a pole, labelled “deuteron” and “Cooper pair”, is bounded by a solid line. The dashed line indicates the momenta for which the energy of a state is $E = 2\mu_F$, and the dotted line the momenta for which $E = 0$. The dash-dotted line is the boundary of a region where the condition (2.28) is satisfied.

with energies $E \leq 2\mu_F$. The $E = 2\mu_F$ boundary is shown as a dashed line. Finally at low densities the matter is unstable against complete deuteronization⁴⁵⁾. The $E = 0$ boundary of the region is shown as a dotted line.

The Cooper pairing is a many-body effect unrelated to the formation of physical deuterons. In our calculation of deuteron production, we only want to include the Green function pole in the “deuteron” region. This can be achieved by imposing a simple condition that a deuteron quasiparticle can only be created when the average nucleon occupation over the phase-space volume corresponding to free-space deuteron wave function, is less than a cutoff value

$$\langle f \rangle_d < f^c = 0.20. \quad (2.28)$$

The boundary of a region where the condition is satisfied is shown as the dot-dashed line in fig. 2. The cutoff value (2.28) corresponds to a 40% removal of the free-space wave-function due to antisymmetrization.

Another discussion of the derivation of a transport equation for composites was given by Röpke and Schulz⁴⁸⁾ who treated the transition matrix elements in the Born approximation and did not consider the effects of statistics. General references on the topic are refs.^{49,50)}.

3. Production and absorption rates

The lowest-order contributions to deuteron production and absorption rates, illustrated in fig. 3a, correspond to the formation and dissolution of deuterons by the interaction of proton and neutron quasiparticles. This is just the mechanism of low-energy (p, d) nuclear reactions⁵¹⁾ where the proton quasiparticle is the distorted projectile wave function and the neutron quasiparticle is a shell-model orbital. This

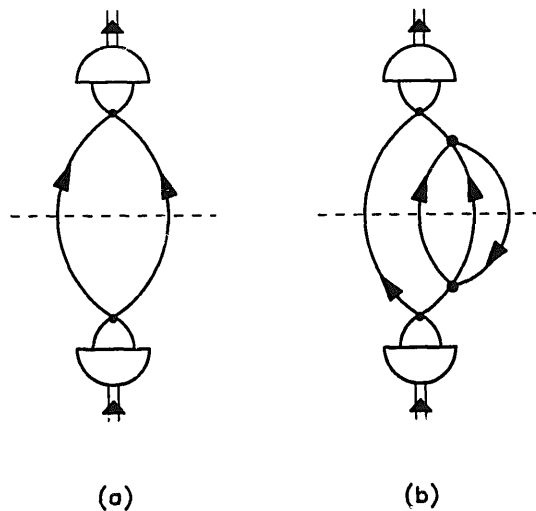


Fig. 3. Expansion of deuteron production and absorption rates. The lines indicate here quasiparticle contributions to the functions only, in distinction to fig. 1. For more details see ref.⁴²⁾. Production or absorption in proton-neutron interaction (a) and in three-nucleon interaction (b).

process requires momentum and energy matching between the deuteron and nucleon quasiparticles, which becomes difficult to fulfill⁵¹⁾ as the incident energy is increased. In infinite matter, when quasiparticles have definite momenta and energies, the binary contributions to the rates would be identically zero, unless energy shifts were such that the deuteron entered two-nucleon continuum. Close to the threshold the phase space for the processes would be low.

A less restrictive mechanism for the production and destruction of deuterons is via the three-nucleon interactions. The lowest-order contributions obtained from the insertion of (2.26) into \mathcal{G}^D , are illustrated in fig. 3b. Further contributions of the same order in two-body scattering matrix, required by antisymmetrization, come from \mathcal{G}^C . The production process illustrated in fig. 3b is such that a nucleon is off-shell after a binary collision, and is capable of forming a deuteron with another nucleon. We shall assume that the three-nucleon collisions are responsible for the deuteron formation in the energetic heavy-ion collisions.

On isolating specific contributions in the quasiparticle expansion of production and absorption rates^{42,52)} averaged over spin directions, we find the following deuteron production rate,

$$\begin{aligned}
 \mathcal{K}_d^<(\mathbf{P}) = & \frac{3m_d}{E(\mathbf{P})} \int \frac{d\mathbf{P}_1}{(2\pi)^3} \frac{m_d}{E(\mathbf{P}_1)} \int \frac{d\mathbf{P}'}{(2\pi)^3} \frac{m_d}{E(\mathbf{P}')} \int \frac{d\mathbf{P}'_1}{(2\pi)^3} \frac{m_d}{E(\mathbf{P}'_1)} \frac{1}{2} |\overline{\mathcal{M}_{dd \rightarrow dd}}|^2 \\
 & \times (2\pi)^3 \delta(\mathbf{P} + \mathbf{P}_1 - \mathbf{P}' - \mathbf{P}'_1) 2\pi \delta(E(\mathbf{P}) + E(\mathbf{P}_1) - E(\mathbf{P}') - E(\mathbf{P}'_1)) \\
 & \times (1 + f_d(\mathbf{P}_1)) f_d(\mathbf{P}') f_d(\mathbf{P}'_1) + \frac{2m_d}{E(\mathbf{P})} \sum_{N=n,p} \int \frac{d\mathbf{p}}{(2\pi)^3} \frac{m_N}{e(\mathbf{p})} \int \frac{d\mathbf{P}'}{(2\pi)^3} \\
 & \times \frac{m_d}{E(\mathbf{P}')} \int \frac{d\mathbf{p}'}{(2\pi)^3} \frac{m_N}{e(\mathbf{p}')} |\overline{\mathcal{M}_{dN \rightarrow dN}}|^2 (2\pi)^3 \delta(\mathbf{P} + \mathbf{p} - \mathbf{P}' - \mathbf{p}') \\
 & \times 2\pi \delta(E(\mathbf{P}) + e(\mathbf{p}) - E(\mathbf{P}') - e(\mathbf{p}')) (1 - f(\mathbf{p})) f_d(\mathbf{P}'_1) f_N(\mathbf{p}') \\
 & + \frac{8}{3} \frac{m_d}{E_d(\mathbf{P})} \sum_{N=n,p} \int \frac{d\mathbf{p}}{(2\pi)^3} \frac{m_N}{e(\mathbf{p})} \int \frac{d\mathbf{p}'_1}{(2\pi)^3} \frac{m_N}{e(\mathbf{p}'_1)} \int \frac{d\mathbf{p}'_2}{(2\pi)^3} \frac{m_N}{e(\mathbf{p}'_2)} \\
 & \times \int \frac{d\mathbf{p}'}{(2\pi)^3} \frac{m_N}{e(\mathbf{p}')} \frac{1}{2} |\overline{\mathcal{M}_{pnN \rightarrow dN}}|^2 (2\pi)^3 \delta(\mathbf{P} + \mathbf{p} - \mathbf{p}'_1 - \mathbf{p}'_2 - \mathbf{p}') \\
 & \times 2\pi \delta(E(\mathbf{P}) + e(\mathbf{p}) - e(\mathbf{p}'_1) - e(\mathbf{p}'_2) - e(\mathbf{p}')) (1 - f_N(\mathbf{p})) \\
 & \times f_p(\mathbf{p}'_1) f_n(\mathbf{p}'_2) f_N(\mathbf{p}') + \dots, \tag{3.1}
 \end{aligned}$$

and the corresponding deuteron absorption rate,

$$\begin{aligned}
 \mathcal{K}_d^>(\mathbf{P}) = & \dots + \frac{2m_d}{E_d(\mathbf{P})} \sum_{N=n,p} \int \frac{d\mathbf{p}}{(2\pi)^3} \frac{m_N}{e(\mathbf{p})} \int \frac{d\mathbf{p}'_1}{(2\pi)^3} \frac{m_N}{e(\mathbf{p}'_1)} \int \frac{d\mathbf{p}'_2}{(2\pi)^3} \frac{m_N}{e(\mathbf{p}'_2)} \\
 & \times \int \frac{d\mathbf{p}'}{(2\pi)^3} \frac{m_N}{e(\mathbf{p}')} \frac{1}{2} |\overline{\mathcal{M}_{dN \rightarrow pnN}}|^2 (2\pi)^3 \delta(\mathbf{P} + \mathbf{p} - \mathbf{p}'_1 - \mathbf{p}'_2 - \mathbf{p}') \\
 & \times 2\pi \delta(E(\mathbf{P}) + e(\mathbf{p}) - e(\mathbf{p}'_1) - e(\mathbf{p}'_2) - e(\mathbf{p}')) f_N(\mathbf{p}) \\
 & \times (1 - f_p(\mathbf{p}'_1)) (1 - f_n(\mathbf{p}'_2)) (1 - f_N(\mathbf{p}')) + \dots. \tag{3.2}
 \end{aligned}$$

These equations look rather imposing, but in fact are nothing more than Fermi's golden rule with matrix elements and phase space integrals cast into a Lorentz-covariant form. The three terms at the r.h.s. of (3.1) represent the dd and dN scattering, and the deuteron production in three-nucleon collisions. These processes are shown schematically in fig. 4. In (3.2) we indicate only a term corresponding to the deuteron breakup in interactions with nucleons. All functions in (3.1) and (3.2) refer to a time T and location \mathbf{R} . The energies e are nucleon single-particle energies. We have introduced in (3.1) and (3.2) factors m/E appropriate in the relativistic case⁵³⁻⁵⁵), otherwise putting the quasiparticle strength equal to 1. The factors $|\overline{\mathcal{M}}|^2$ stand for matrix elements squared summed over the final and averaged over the initial spin directions. The numeric factors in front of each of the terms on the r.h.s. of eqs. (3.1) and (3.2) arise from the process of summation and averaging over the spin indices. The process of deuteron formation in three-nucleon collisions is inverse to the deuteron breakup, and we have

$$|\overline{\mathcal{M}}_{pnN \rightarrow dN}|^2 = \frac{3}{4} |\overline{\mathcal{M}}_{dN \rightarrow pnN}|^2. \quad (3.3)$$

More generally, matrix elements are related by

$$|\overline{\mathcal{M}}_{i \rightarrow f}|^2 = (g_f/g_i) |\overline{\mathcal{M}}_{f \rightarrow i}|^2. \quad (3.4)$$

where g_k is the spin degeneracy factor in channel k . In the context of (p, pd) reactions, the relation between deuteron formation and breakup has been discussed by Lovas⁵⁶).

The terms involving nucleons in eqs. (3.1) and (3.2) have counterparts in the formulas for nucleon absorption and production rates¹⁸). Thus, writing the neutron transport equation as

$$\frac{\partial f_n}{\partial T} + \frac{\partial e}{\partial \mathbf{p}} \cdot \frac{\partial f_n}{\partial \mathbf{R}} - \frac{\partial e}{\partial \mathbf{R}} \cdot \frac{\partial f_n}{\partial \mathbf{p}} = -i\Sigma_n^<(1-f_n) - i\Sigma_n^>f_n, \quad (3.5)$$

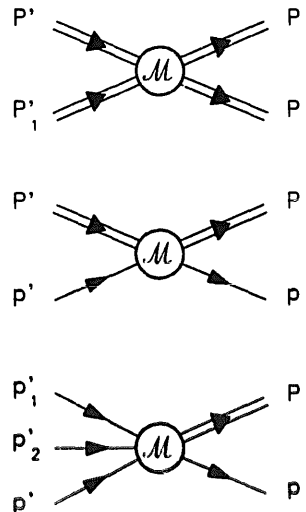


Fig. 4. Processes accounted for at the r.h.s. of eq. (3.1).

the neutron absorption rate has a term corresponding to the third term at the r.h.s. of (3.1), in addition to one associated with NN scattering,

$$\begin{aligned}
 i\Sigma_n^>(\mathbf{p}) = & \dots + \frac{2m_N}{e(\mathbf{p})} \int \frac{d\mathbf{p}_1}{(2\pi)^3} \frac{m_N}{e(\mathbf{p}_1)} \int \frac{d\mathbf{p}'}{(2\pi)^3} \frac{m_N}{e(\mathbf{p}')} \int \frac{d\mathbf{p}'_1}{(2\pi)^3} \frac{m_N}{e(\mathbf{p}'_1)} \\
 & \times \frac{1}{2} |\overline{\mathcal{M}_{nn \rightarrow nn}}|^2 (2\pi)^3 \delta(\mathbf{p} + \mathbf{p}_1 - \mathbf{p}' - \mathbf{p}'_1) 2\pi \delta(e(\mathbf{p}) + e(\mathbf{p}_1) \\
 & - e(\mathbf{p}') - e(\mathbf{p}'_1)) f_n(\mathbf{p}_1)(1 - f_n(\mathbf{p}'))(1 - f_n(\mathbf{p}'_1)) \\
 & + \frac{4m_N}{e(\mathbf{p})} \int \frac{d\mathbf{p}_1}{(2\pi)^3} \frac{m_N}{e(\mathbf{p}_1)} \int \frac{d\mathbf{p}_2}{(2\pi)^3} \frac{m_N}{e(\mathbf{p}_2)} \int \frac{d\mathbf{p}'}{(2\pi)^3} \frac{m_N}{e(\mathbf{p}')} \int \frac{d\mathbf{P}'}{(2\pi)^3} \\
 & \times \frac{m_d}{E(\mathbf{P}')} |\overline{\mathcal{M}_{nnp \rightarrow nd}}|^2 (2\pi)^3 \delta(\mathbf{p} + \mathbf{p}_1 + \mathbf{p}_2 - \mathbf{p}' - \mathbf{P}') \\
 & \times 2\pi \delta(e(\mathbf{p}) + e(\mathbf{p}_1) + e(\mathbf{p}_2) - e(\mathbf{p}') - E(\mathbf{P}')) \\
 & \times f_n(\mathbf{p}_1) f_p(\mathbf{p}_2)(1 - f_n(\mathbf{p}'))(1 + f_d(\mathbf{P}')) .
 \end{aligned} \quad (3.6)$$

Collision processes in (3.1), (3.2), and (3.6), would eventually lead to equilibrium distributions given, in a local rest-frame, by

$$f_N(\mathbf{p}) = 1/[\exp(\beta(e(\mathbf{p}) - \mu_N)) + 1] , \quad (3.7)$$

$$f_d(\mathbf{P}) = 1/[\exp(\beta(E(\mathbf{P}) - \mu_d)) - 1] , \quad (3.8)$$

with $\mu_d = \mu_n + \mu_p$, and β - the inverse temperature.

It may be useful to have some visualization for the three-body collision processes. When there are two particles in the initial state of a collision, the rate is conveniently expressed in terms of a cross section. The formula, obtained by integrating over final states, reads

$$\int dP_f (m_1/e_1)(m_2/e_2) |\overline{\mathcal{M}_{12 \rightarrow f}}|^2 (2\pi)^3 \delta(\mathbf{P}_{12} - \mathbf{P}_f) 2\pi \delta(E_{12} - E_f) = \sigma v_{12} . \quad (3.9)$$

On the l.h.s., dP_f stands for the integration over final momenta with appropriate $m/(2\pi)^3 e$ and symmetry factors, \mathbf{P} and E are total momentum and energy in the initial and final state, and we have dropped statistical factors. The result of the integration over the transition element squared has a dimension of the area times velocity; with v_{12} - relative velocity, eq. (3.9) defines the interaction cross section σ . One can imagine that a transition occurs once the particles find themselves within the relative distance r such that $\pi r^2 = \sigma$. In the three-body case the result of an analogous integration has a dimension of volume times area times velocity,

$$\int dP_f \frac{m_1}{e_1} \frac{m_2}{e_2} \frac{m_3}{e_3} |\overline{\mathcal{M}_{123 \rightarrow f}}|^2 (2\pi)^3 \delta(\mathbf{P}_{123} - \mathbf{P}_f) 2\pi \delta(E_{123} - E_f) = \mathcal{V} \mathcal{J} v . \quad (3.10)$$

If one takes the velocity v as the relative velocity of 1 and 2, e.g. in the overall center-of-mass, then one can suppose that the transition occurs once 1 and 2 find

themselves within the distance corresponding to the area \mathcal{S} from one another, providing 3 is within the volume \mathcal{V} from the geometric or mass center of 1 and 2. This is depicted in fig. 5. The radii of \mathcal{S} and \mathcal{V} may be taken to be similar. The analysis is easily extended to processes involving more bodies. An n -body collision rate may be represented as $\mathcal{V}^{n-2}\mathcal{S}v$, and the transition may be considered to occur if the $(n-2)$ bodies are within \mathcal{V} from the center of 1 and 2.

In evaluating the rates for nucleon-nucleon scattering, the most straightforward procedure is to use the free-space cross-sections

$$\frac{m_N^4}{16\pi^2 e^{*2}} \overline{|\mathcal{M}_{NN' \rightarrow NN'}|^2} = \frac{d\sigma_{NN' \rightarrow NN'}}{d\Omega^*}, \quad (3.11)$$

where e^* is c.m. nucleon energy. The matrix element for deuteron production and breakup might, in principle, be also taken from data using the formula

$$\frac{1}{64\pi^5} \frac{m_N^4 m_d}{p^*(e^* + E^*)} \frac{p_1^{**}}{e_1^{**} e_3^*} \overline{|\mathcal{M}_{pd \rightarrow ppn}|^2} = \frac{d\sigma_{pd \rightarrow ppn}}{d\Omega_1^{**} d^3 p_3^*}. \quad (3.12)$$

The quantities with superscript “*” in (3.12) are in the overall center-of-mass, and those with “**” are in the center-of-mass of particles 1 and 2 in the final state. Because of the many variables in the three-body phase space, the differential cross sections are known only for a limited range of final states. We shall therefore use a simple impulse model covering the entire kinematic region.

The lowest-order nonvanishing contributions to the deuteron production and absorption rates are obtained from eqs. (2.25), (2.5), and (2.26), using the T -matrix approximation^{41,18)} to Σ . The contributions are illustrated in fig. 3b. When effects of antisymmetrization with particles in the medium are ignored, the product of Green function, interaction potential, and wave function in the deuteron frame (cf. eq. (2.25)), produces the wave function⁴⁷⁾, and we get

$$\begin{aligned} \overline{|\mathcal{M}_{pd \rightarrow ppn}|^2}_{IA} \approx & |\langle \tilde{p}_1 | \phi \rangle|^2 \overline{|\mathcal{M}_{pn \rightarrow pn}|^2} + |\langle \tilde{p}_2 | \phi \rangle|^2 \overline{|\mathcal{M}_{pn \rightarrow pn}|^2} \\ & + |\langle \tilde{p}_3 | \phi \rangle|^2 \overline{|\mathcal{M}_{pp \rightarrow pp}|^2}. \end{aligned} \quad (3.13)$$

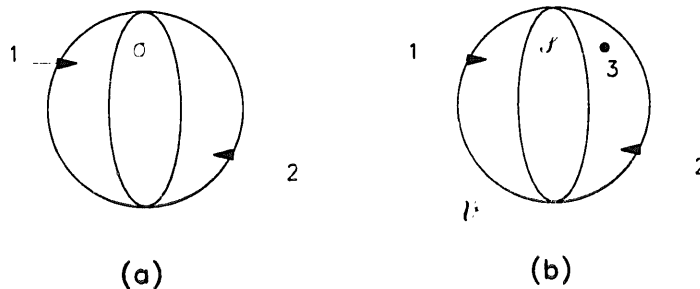


Fig. 5. Two-body (a) and three-body (b) collision. Transition may be considered to occur once the particles find themselves within a specified distance.

$$|\overline{\mathcal{M}}_{\text{Nd} \rightarrow \text{Npn}}|_{\text{IA}}^2 = \left| \begin{array}{c} \text{Diagram 1} \\ \text{Diagram 2} \\ \text{Diagram 3} \end{array} \right|^2 + \left| \begin{array}{c} \text{Diagram 4} \\ \text{Diagram 5} \\ \text{Diagram 6} \end{array} \right|^2 + \left| \begin{array}{c} \text{Diagram 7} \\ \text{Diagram 8} \\ \text{Diagram 9} \end{array} \right|^2$$

Fig. 6. Matrix element squared for deuteron breakup in the impulse approximation, see text. The element for deuteron formation may be represented with the direction of lines inverted.

This is just the impulse approximation, fig. 6, with direct terms only. We use tilde to indicate vectors in the deuteron center-of-mass in (3.13). The wave function is normalized so that

$$\int \frac{d\mathbf{p}}{(2\pi)^3} |\langle \mathbf{p} | \phi \rangle|^2 = 1. \quad (3.14)$$

The impulse approximation is expected to work well at high energies.

The two-nucleon matrix elements in (3.13) may be related to the NN cross section using (3.11). The cross section is evaluated at an energy in the two-nucleon system equal to that of the pair in the final state. An expression for the deuteron breakup cross section then becomes

$$\begin{aligned} \sigma_{\text{pd} \rightarrow \text{ppn}}^{\text{IA}} &= \frac{1}{2\pi^2} \frac{m_d^2}{p^{*2}(e^* + E^*)} \int_0^{p_3^{*\text{max}}} dp_3^* \frac{p_3^* p_1^{**} e_1^{**}}{e_3^*} (\sigma_{\text{pp} \rightarrow \text{pp}} + \sigma_{\text{pn} \rightarrow \text{pn}}) \\ &\times \int_{\tilde{p}_3^{\text{min}}}^{\tilde{p}_3^{\text{max}}} d\tilde{p}_3 \frac{\tilde{p}_3}{\tilde{e}_3} |\langle \tilde{\mathbf{p}}_3 | \phi \rangle|^2. \end{aligned} \quad (3.15)$$

Nucleon 3 in (3.15) is the spectator. In fig. 7 we show the ratio F of the measured Nd inelastic cross to the cross section in the impulse approximation (3.15) using

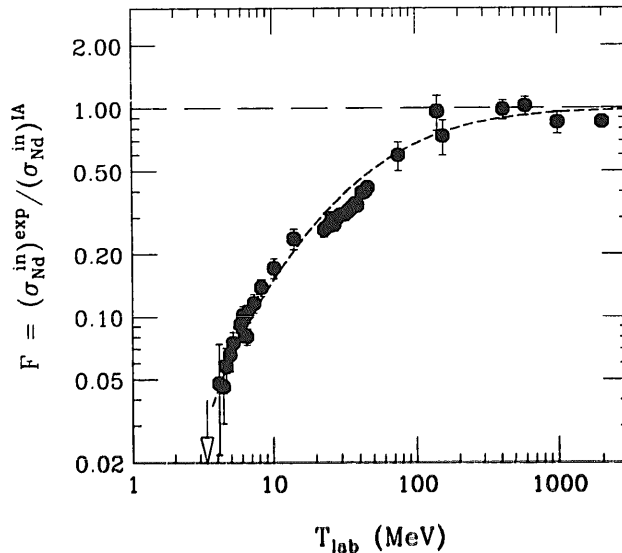


Fig. 7. Ratio of the measured inelastic Nd cross section to the cross section in the impulse approximation.

the total NN cross sections. The ratio tends to 1 for high energies and falls below $\frac{1}{20}$ close to threshold. In our numerical calculations we take the values of experimental Nd cross sections from refs. ⁵⁷⁻⁶¹), NN cross sections from refs. ⁶¹⁻⁶³), and deuteron momentum distribution such as in ref. ⁴⁷).

We compensate for the failure of the impulse model at low energies by multiplying $|\mathcal{M}|_{IA}^2$ by the ratio F ,

$$|\mathcal{M}_{Nd \rightarrow Npn}|^2 = F |\mathcal{M}_{Nd \rightarrow Npn}|_{IA}^2. \quad (3.17)$$

In the energy range of interest we can approximate F with

$$F \simeq \frac{\delta + 1}{\delta + 32}, \quad (3.18)$$

where $\delta = e^* + E^* - 3m_N$ in MeV. This is indicated with a short-dashed line in fig. 7. The NN matrix elements in $|\mathcal{M}_{NN' \rightarrow NN'}|^2$ in (3.13) are taken to be isotropic for simplicity.

Eq. (3.3) plays a similar role as the detailed balance relation in case when there are two particles in initial and final states. It ensures, in particular, a proper form of the thermodynamic equilibrium distributions. With (3.3), (3.17), (3.13) and (3.11), the deuteron formation rate (3.10) may be written as

$$\begin{aligned} & \int \frac{d\mathbf{p}}{(2\pi)^3} \int \frac{d\mathbf{P}}{(2\pi)^3} \frac{m_N^3}{e(\mathbf{p}_1)e(\mathbf{p}_2)e(\mathbf{p}_3)} \frac{m_N m_d}{e(\mathbf{p})E(\mathbf{P})} |\mathcal{M}_{ppn \rightarrow pd}|^2 \\ & \times (2\pi)^3 \delta(\mathbf{p}_1 + \mathbf{p}_2 + \mathbf{p}_3 - \mathbf{p} - \mathbf{P}) 2\pi \delta(e(\mathbf{p}_1) + e(\mathbf{p}_2) + e(\mathbf{p}_3) - e(\mathbf{p}) - E(\mathbf{P})) \\ & = v_{12} 2\sigma_{pp \rightarrow pp} \mathcal{V}_3 + v_{13} \sigma_{pn \rightarrow pn} \mathcal{V}_2 + v_{23} \sigma_{pn \rightarrow pn} \mathcal{V}_1, \end{aligned} \quad (3.19)$$

with volume

$$\begin{aligned} \mathcal{V}_3 &= F \frac{3}{4} \frac{2p^* m_d e_1^{**}}{p_1^{**}(e^* + E^*) e_3} \int \frac{d\Omega^*}{4\pi} |\langle \tilde{\mathbf{p}}_3 | \phi \rangle|^2 \\ &= F \frac{3}{4} \frac{m_d^2 e_1^{**}}{p_1^{**}(e^* + E^*) p_3^* e_3} \int d\tilde{\mathbf{p}}_3 \frac{\tilde{\mathbf{p}}_3}{\tilde{e}_3} |\langle \tilde{\mathbf{p}}_3 | \phi \rangle|^2. \end{aligned} \quad (3.20)$$

The physical interpretation of the rate formula is that a nucleon will form a deuteron after an NN collision only if it finds a partner within the momentum-dependent volume \mathcal{V} given by (3.20). The various factors in the r.h.s. of the first equality in (3.20) have the following significance: the factor $\frac{3}{4}$ is for spin, next in front of the integral is the ratio of fluxes and kinematic factors, finally, for low spectator momenta the square of the momentum-space wave function is of the order of spatial volume of a deuteron.

For elastic Nd interactions, we use isotropic cross sections in our numerical calculations. The dd interactions are treated as entirely elastic, with the cross sections assumed to be twice the pd cross sections at half the bombarding energy. The angular dependence of NN elastic differential cross sections is taken to be the same as in ref. ¹⁷).

4. Pion production

Pion production in heavy-ion reactions has been a subject of controversy over the years¹⁹⁻²²), with fewer pions observed than predicted by the cascade model. In cascade and other dynamic descriptions of energetic heavy-ion reactions, pion production is usually treated via the formation of Δ -resonances in NN collisions^{14-17,24-32}). [N^* resonances have also been considered^{33,34}).] The resonances may be reabsorbed in the collisions with nucleons, or eventually they decay into nucleons and pions. Decays occur after the completion of the heavy-ion reaction^{15-17,24,30}), or during the reaction^{24-27,29,33,34}). Pions may possibly form resonances when interacting with nucleons^{24-29,33,34}). In these references, the resonance reabsorption cross sections are taken from the detailed balance relation of the form^{17,64}), for the Δ ,

$$\sigma_{N\Delta \rightarrow NN} = \frac{p^{*2}}{8p'^{*2}} \sigma_{NN \rightarrow N\Delta} . \quad (4.1)$$

Here p'^* and p^* are the c.m. momenta in the $N\Delta$ channel and in the NN channel, respectively. Cross sections are averaged over the spin and isospin values in the initial state and summed over final states. The variable resonance masses are selected from a Breit-Wigner distribution in many calculations^{16,17,25-34}).

In fact, eq. (4.1) is not valid when the resonance is broad; we shall now derive a cross section formula which applies to broad resonances as well. This will considerably ameliorate the discrepancy between cascade results and experiment.

The nucleon absorption rate includes a term associated with resonance formation which may be written as

$$\begin{aligned} i\Sigma_n^>(p) = & \dots + \frac{2m_N}{e(p)} \sum_r \int \frac{d\mathbf{p}_1}{(2\pi)^3} \frac{m_N}{e(\mathbf{p}_1)} \int \frac{d\mathbf{p}'}{(2\pi)^3} \frac{m_N}{e(\mathbf{p}')} \int \frac{d\mathbf{p}''}{(2\pi)^3} \int \frac{d\mathcal{E}}{2\pi} \\ & \times |\overline{\mathcal{M}_{np \rightarrow N^*r}}|^2 (2\pi)^3 \delta(\mathbf{p} + \mathbf{p}_1 - \mathbf{p}' - \mathbf{p}'') \\ & \times 2\pi \delta(e(\mathbf{p}) + e(\mathbf{p}_1) - e(\mathbf{p}') - \mathcal{E}) f_p(\mathbf{p}_1) (1 - f_{N^*}(\mathbf{p}')) \\ & \times A_r(\mathbf{p}'', \mathcal{E}) (1 - \ell_r(\mathbf{p}'', \mathcal{E})) + \dots . \end{aligned} \quad (4.2)$$

Here A_r is the spectral function of the resonance, and ℓ_r is an occupation factor for the resonance. Under the conditions of heavy-ion reactions ℓ_r is always small and may be neglected compared to 1. In the vacuum the function A_r is

$$\begin{aligned} A_r &= \frac{4m_r^2 \Gamma_r}{(m^2 - m_r^2)^2 + m_r^2 \Gamma_r^2} \\ &\simeq \frac{\Gamma_r}{(m - m_r)^2 + \frac{1}{4}\Gamma_r^2} , \end{aligned} \quad (4.3)$$

where m_r is the resonance mass, $m^2 = \mathcal{E}^2 - \mathbf{p}^2$, and Γ_r is the width in the center of mass, which in general is dependent on m . When the $N\pi$ channel dominates in the decay, the width is

$$\begin{aligned} \Gamma_r &= \sum_{N'} \Gamma_{r \rightarrow N'\pi} = \sum_{N'} \int \frac{d\mathbf{p}}{(2\pi)^3} \frac{m_N}{e(\mathbf{p})} \int \frac{d\mathbf{p}'}{(2\pi)^3} \frac{m_\pi}{e_\pi(\mathbf{p}')} \overline{|\mathcal{M}_{r \rightarrow N'\pi}|^2} \\ &\quad \times (2\pi)^3 \delta(\mathbf{p} + \mathbf{p}') 2\pi \delta(m - e(\mathbf{p}) - e_\pi(\mathbf{p}')) \\ &= \frac{m_N m_\pi p^*}{\pi m} \sum_{N'} \overline{|\mathcal{M}_{r \rightarrow N'\pi}|^2}. \end{aligned} \quad (4.4)$$

Clearly, the pion production rate has to include a term corresponding to the resonance decay, and the absorption rate a term corresponding to the resonance formation, of the form

$$\begin{aligned} &\frac{m_\pi}{e_\pi(\mathbf{p})} \int \frac{d\mathbf{p}_1}{(2\pi)^3} \frac{m_N}{e(\mathbf{p}_1)} \int \frac{d\mathbf{p}'}{(2\pi)^3} \int \frac{d\mathcal{E}}{2\pi} \overline{|\mathcal{M}_{N\pi \rightarrow r}|^2} (2\pi)^3 \delta(\mathbf{p} + \mathbf{p}_1 - \mathbf{p}') \\ &\quad \times 2\pi \delta(e_\pi(\mathbf{p}) + e(\mathbf{p}_1) - \mathcal{E}) f_N(\mathbf{p}_1) A_r(\mathbf{p}', \mathcal{E}) (1 - \ell_r(\mathbf{p}', \mathcal{E})), \end{aligned} \quad (4.5)$$

for a pion with momentum \mathbf{p} . It is relatively straightforward to show that these results hold under the conditions of thermodynamic equilibrium when the quasiparticle approximations are used for pions and nucleons, cf. refs.^{41,18,65}). General formulae for resonant cross sections are given in ref.⁶⁶). In equilibrium the occupation factors are

$$\ell_r = \frac{1}{e_N p [\beta(\mathcal{E} - \mu_r)] + 1} \approx \exp[\beta(\mu_r - \mathcal{E})], \quad (4.6a)$$

$$f_\pi = \frac{1}{\exp[\beta(e_\pi(\mathbf{p}) - \mu_\pi)] - 1} \approx \exp[\beta(\mu_\pi - e_\pi(\mathbf{p}))], \quad (4.6b)$$

and the chemical potentials satisfy

$$\begin{aligned} \mu_{\Delta^+} &= \mu_{N^{*+}} = \mu_p, & \mu_{\Delta^0} &= \mu_{N^{*0}} = \mu_n, \\ \mu_{\Delta^{++}} &= 2\mu_p - \mu_n, & \mu_{\Delta^-} &= 2\mu_n - \mu_p, \\ \mu_{\mu^+} &= -\mu_{\mu^-} = \mu_p - \mu_n. \end{aligned} \quad (4.7)$$

From (4.7) we find

$$\mu_{\pi^+} - \mu_{\pi^-} = 2(\mu_p - \mu_n), \quad (4.8)$$

and in a low-density system we expect

$$N_{\pi^+}/N_{\pi^-} = (N_p/N_n)^2. \quad (4.9)$$

The results for the rates, (4.2) and (4.5), hold also out of equilibrium when the absorption rates of resonances are large compared to the time variations in the

resonance production and absorption rates. In that limit, with a similar expansion^{41,18)} as in the case of deuterons, we can show that the following equation holds for resonances,

$$\begin{aligned} \frac{\partial}{\partial T} (\ell_r A_r) + \frac{\partial \mathcal{E}}{\partial \mathbf{p}} \cdot \frac{\partial}{\partial \mathbf{R}} (\ell_r A_r) - \frac{\partial \mathcal{E}}{\partial \mathbf{R}} \cdot \frac{\partial}{\partial \mathbf{p}} (\ell_r A_r) \\ = -i\Sigma_r^< (1 - \ell_r) A_r - i\Sigma_r^> \ell_r A_r. \end{aligned} \quad (4.10)$$

Here under the derivatives on the l.h.s. the condition $\Delta m = m - m_r = \text{constant}$ (more generally $\text{Re}(G^+)^{-1} = \text{constant}$) is satisfied. If the dependence of the width in spectral function on space and time is ignored, then the spectral function may be taken out from under the derivatives and factored out from the equation. An example of a term in the rates is

$$\begin{aligned} i\Sigma_r^>(\mathbf{p}, \mathcal{E}) = \dots + \frac{2m}{\mathcal{E}} \int \frac{d\mathbf{p}_1}{(2\pi)^3} \frac{m_N}{e(\mathbf{p}_1)} \int \frac{d\mathbf{p}'}{(2\pi)^3} \frac{m_N}{e(\mathbf{p}')} \int \frac{d\mathbf{p}'_1}{(2\pi)^3} \frac{m_N}{e(\mathbf{p}'_1)} \\ \times \overline{|\mathcal{M}_{nn \rightarrow NN'}|^2} (2\pi)^3 \delta(\mathbf{p} + \mathbf{p}_1 - \mathbf{p}' - \mathbf{p}'_1) 2\pi \delta(\mathcal{E} + e(\mathbf{p}_1) \\ - e(\mathbf{p}') - e(\mathbf{p}'_1)) f_n(\mathbf{p}_1) (1 - f_N(\mathbf{p}')) \\ \times (1 - f_N(\mathbf{p}'_1)) + \dots \end{aligned} \quad (4.11)$$

Let us now discuss some consequences of the above results. With (4.2), the differential cross section for the production of a resonance with mass m becomes

$$\frac{d\sigma_{NN' \rightarrow N''r}}{d\Omega^* dm} = \frac{m_N^3}{32\pi^3 e^{*2}} \frac{p'^*}{p^*} \overline{|\mathcal{M}_{NN' \rightarrow N''r}|^2} m A_r. \quad (4.12)$$

Here e^* and p^* are the nucleon c.m. energy and momentum in the NN channel, and p'^* is the c.m. momentum in the Nr channel. To the extent that the variation of $|\mathcal{M}|^2$ with m may be ignored^{67,68)} the resonance mass should be sampled using the function

$$p'^* m A_r(m), \quad (4.13)$$

rather than A_r , as was done in refs.^{16,17,25-34)}. Consequently the masses m close to the maximum $2e^* - m_N$ get suppressed. The full cross section for the resonance production becomes

$$\sigma_{NN' \rightarrow N''r} = \frac{m_N^3}{4\pi e^{*2} p^*} \int_{m_N + m_\pi}^{2e^* - m_N} \frac{dm}{2\pi} m A_r p'^* \int \frac{d\Omega^*}{4\pi} \overline{|\mathcal{M}_{NN' \rightarrow N''r}|^2}, \quad (4.14)$$

and the cross section for resonance absorption is, following (4.11),

$$\sigma_{N''r \rightarrow NN'} = \frac{m_N^3 m}{4\pi e^{*2}} \frac{p^*}{p'^*} \frac{1}{1 + \delta_{NN'}} \int \frac{d\Omega^*}{4\pi} \overline{|\mathcal{M}_{N''r \rightarrow NN'}|^2}. \quad (4.15)$$

From eq. (3.4), the cross sections for the two reactions can be made proportional to one another, if the dependence of $|\mathcal{M}|^2$ on m is neglected. In the case of Δ , we

find for the isospin-averaged cross section the result,

$$\sigma_{N\Delta \rightarrow NN} = \frac{1}{8} \frac{mp^{*2}}{p'^{*2}} \sigma_{NN \rightarrow N\Delta} / \int \frac{dm''}{2\pi} m'' A_{\Delta}(m'') p^{*2}. \quad (4.16)$$

The range of integration over the mass is the same as in (4.14).

Let us discuss the significance of the difference between (4.16) and (4.1). Thermal equilibrium is established when the rates of production and absorption balance. In the processes of the resonance formation and absorption in heavy-ion collisions, the c.m. energies close to threshold are most important, because temperatures do not exceed the order of magnitude of the pion mass. The cross sections for resonance absorption from (4.16) are larger, on the average, than cross sections from (4.1), due to the division in the r.h.s. of (4.16) by the integral over the portion of spectral function. Eq. (4.1) is derived assuming that density of states in the $N\Delta$ channel is such as for two stable particles, disregarding the spread of Δ in energy. If Δ -reabsorption cross section is underestimated by a factor of 2, then, up to second-order effects, the total number of Δ 's and pions will be overestimated, in equilibrium, by a factor of 2, in comparison to (4.6) and (4.7). The average factor is expected to be largest for the low temperatures or bombarding energy, and decrease with the increase in energy. The reabsorption cross sections are of lesser significance for light systems and large impact parameters than for heavier systems and small impact parameters.

The cross section for resonance formation in $N\pi$ interaction is, with (4.5),

$$\sigma_{N\pi \rightarrow r} = \frac{m_{\pi} m_N}{mp^{*2}} |\mathcal{M}_{N\pi \rightarrow r}|^2 A_r(m) = \frac{\pi}{p^{*2}} \frac{g_r}{2} \Gamma_{r \rightarrow N\pi} A_r, \quad (4.17)$$

and in obtaining the last standard⁶⁶⁾ result we use (3.4) and (4.4).

The numerical calculations are carried out with the isospin components of multiplets made explicit. For the Δ width we take^{69,70,33)}

$$\Gamma_{\Delta} = \frac{2}{3} \frac{f_{\Delta}^2}{4\pi} \frac{m_N}{m_{\pi}^2} \frac{p^{*3}}{m} \left(\frac{\beta^2 + p_{\Delta}^{*2}}{\beta^2 + p^{*2}} \right)^2, \quad (4.18)$$

with $f_{\Delta}^2/4\pi = 0.37$, $\beta = 300$ MeV/c, and for the N^* width⁷¹⁾

$$\Gamma_{N^*} = \Gamma_{N^*}^0 (p^*/p_{N^*}^*)^3, \quad (4.19)$$

where $\Gamma_{N^*}^0 = 200$ MeV. The NN scattering data^{61,68)} are used to obtain the cross sections for resonance production. For high energies, corresponding to $T_{lab} \geq 0.9$ GeV, we use

$$\sigma_{pn \rightarrow nN^{*+}} \simeq \frac{1}{2} \sigma_{pn}^{inel} - \frac{1}{4} \sigma_{pp}^{inel}, \quad (4.20)$$

and for lower energies the parametrization by VerWest and Arndt⁶⁸⁾, taking

$$\sigma_{pn \rightarrow nN^{*+}} = \frac{3}{4} \sigma_{01}. \quad (4.21)$$

For the excitation to Δ -resonances at high energies we use⁶⁸⁾,

$$\sigma_{pp \rightarrow n\Delta^{++}} = \sigma_{pp}^{inel} (\sigma_{10} + \frac{1}{2} \sigma_{11}) / (2\sigma_{11} + \sigma_{10}), \quad (4.22a)$$

$$\sigma_{pp \rightarrow p\Delta^+} = \sigma_{pp}^{\text{inel}} \frac{3}{2} \sigma_{11} / (2\sigma_{11} + \sigma_{10}), \quad (4.22b)$$

$$\sigma_{pn \rightarrow p\Delta^0} = \frac{1}{2} \sigma_{pp}^{\text{inel}}, \quad (4.22c)$$

and at low energies we replace $\sigma_{pp}^{\text{inel}}$ in (4.22) by $2\sigma_{11} + \sigma_{10} + \sigma_{10}^d$. The angular dependence of the cross section is the same as determined in ref. ³³).

We conclude this section with some general remarks about the transport approach to pion production. When the delta absorption rate is large compared to the rate of variation of the production of resonances, the processes of resonance production and absorption nearly balance. The r.h.s. of eq. (4.10) is close to zero, and the equation describes the shifting of an equilibrium distribution under the changes in the production and absorption rates. The delta decay rate may not be high enough to satisfy this quasi-equilibrium condition when the mass is close to the decay threshold. Still the Δ -resonance functions may be the equilibrium ones (with respect to processes of production and absorption, and not necessarily thermodynamic), because the Δ is mainly virtual in this situation and a much shorter time scale applies to virtual particles. The other sufficient condition for the equilibrium is that $|m - m_\Delta|$ is large compared to the time variation of the production rate. While eq. (4.10) can be violated, the equilibrium Δ -resonance functions might still be used in the nucleon and pion rates. It appears then, that because of equilibrium, one can eliminate the Δ -occupations entirely, and treat the $NN\pi$ states explicitly as final and initial states of interactions ⁷²), in a similar manner as NNN states in sect. 3. This goes beyond the present paper.

Since we have discussed here pion production, we should mention recent works by Siemens *et al.* ⁷³) and Wang *et al.* ⁷⁴). We found out that transport theory with resonances has been postulated before by Mrówczyński ⁷⁵).

5. Quasiparticle energies

The relativistic version of phenomenological Landau theory, developed by Baym and Chin ⁷⁶), may be used as a guidance in parametrizing the quasiparticle energies. We assume that particle masses are independent of momenta. We take

$$m_N = m_{N0} + U, \quad e(p) = (p^2 + m_N^2)^{1/2}, \quad (5.1)$$

for nucleons,

$$m_d = m_{d0} + 2U, \quad E(P) = (P^2 + m_d^2)^{1/2}, \quad (5.2)$$

for deuterons, and

$$m_r = m_{r0} + U, \quad m = m_r + \Delta m, \quad \mathcal{E}(p, \Delta m) = (p^2 + m^2)^{1/2}, \quad (5.3)$$

for the resonances in transport equations. In the above “0” denotes vacuum masses, $m_{\Delta 0} = 1232 \text{ MeV}/c^2$, $m_{N^*0} = 1440 \text{ MeV}/c^2$, and U is scalar potential

$$U = U(\rho), \quad (5.4)$$

with

$$\begin{aligned} \rho_s = & 2 \int \frac{d\mathbf{p}}{(2\pi)^3} \frac{m_{N0}}{e(\mathbf{p})} (f_p(\mathbf{p}) + f_n(\mathbf{p})) + 6 \int \frac{d\mathbf{P}}{(2\pi)^3} \frac{m_{d0}}{E(\mathbf{P})} f_d(\mathbf{P}) \\ & + \sum_r g_r \int \frac{d\mathbf{p}}{(2\pi)^3} \int \frac{d\mathcal{E}}{2\pi} \frac{m_{r0}}{m} \ell_r(\mathbf{p}, \mathcal{E}) A_r(\mathbf{p}, \mathcal{E}). \end{aligned} \quad (5.5)$$

The pion energies are the same as in free space. The last term in (5.5) is associated with resonances and may be rewritten as

$$\sum_r g_r \int \frac{d\mathbf{p}}{(2\pi)^3} \int \frac{d\Delta m}{2\pi} \frac{m_{r0}}{\mathcal{E}} \ell_r(\mathbf{p}, \Delta m) A_r(\mathbf{p}, \Delta m). \quad (5.6)$$

The energy ⁷⁶⁾ corresponding to (5.1)–(5.6) is

$$\begin{aligned} \mathbb{E} = & \int_0^1 d\lambda \int d\mathbf{r} \left[2 \int \frac{d\mathbf{p}}{(2\pi)^3} e(\mathbf{p}, \lambda) (f_p(\mathbf{p}) + f_n(\mathbf{p})) + 6 \int \frac{d\mathbf{P}}{(2\pi)^3} E(\mathbf{P}, \lambda) f_d(\mathbf{P}) \right. \\ & \left. + \sum_r g_r \int \frac{d\mathbf{p}}{(2\pi)^3} \int \frac{d\Delta m}{2\pi} \mathcal{E}(\mathbf{p}, \Delta m, \lambda) \ell_r(\mathbf{p}, \Delta m) A_r(\mathbf{p}, \Delta m) \right] \\ \simeq & \int d\mathbf{r} \left[2 \int \frac{d\mathbf{p}}{(2\pi)^3} e_0(\mathbf{p}) (f_p(\mathbf{p}) + f_n(\mathbf{p})) + 6 \int \frac{d\mathbf{P}}{(2\pi)^3} E_0(\mathbf{P}) f_d(\mathbf{P}) \right. \\ & \left. + \sum_r g_r \int \frac{d\mathbf{p}}{(2\pi)^3} \int \frac{d\Delta m}{2\pi} \mathcal{E}_0(\mathbf{p}, \Delta m) \ell_r(\mathbf{p}, \Delta m) A_r(\mathbf{p}, \Delta m) + \int_0^{\rho_s} d\rho'_s U(\rho'_s) \right]. \end{aligned} \quad (5.7)$$

The subscript “0” in (5.7) denotes energies calculated with free-space masses. The first three terms at the r.h.s. of (5.7) represent the kinetic energy, and the last term the potential energy.

The dependence of the potential on density is taken the same as in nonrelativistic calculations ^{16,17)}, i.e.

$$U(\rho_s) = A(\rho_s/\rho_s^0) + B(\rho_s/\rho_s^0)^\sigma. \quad (5.8)$$

The case of $A = -356$ MeV, $B = 303$ MeV, $\sigma = \frac{7}{6}$, correspond to the soft equation of state, and $A = -124$ MeV, $B = 70.5$ MeV, $\sigma = 2$, to the stiff equation; $\rho_s^0 \approx \rho^0 \approx 0.145 \text{ fm}^{-3}$. Unless explicitly stated, the results of calculations are for the first set of parameters.

6. Numerical results

The method of solving the set of coupled transport equations for nucleons, deuterons, nucleon resonances, and pions is described in the appendix. We first compare results for the particle yields in energetic heavy-ion reactions with data. These are summarized in table 1. Auble *et al.* ³⁸⁾ have determined the yields at all angles above their energy thresholds, which is 15 MeV for p and 21 MeV for d. The calculated yields given in the table are integrated over energies above these thresholds. We should mention that the deuteron yield is, in general, sensitive to the cut-off

TABLE 1
Particle yields from heavy-ion induced reactions

Reaction		Yield (b)						
		p	d	^3H	^3He	α	π^+	π^-
O + Ni	exp.	4.62	2.04	0.87	0.71	2.0		
100 MeV/nucleon	soft	7.16	3.38					
Na + NaF	exp.	3.9	1.2	0.19	0.17		0.077	0.086
400 MeV/nucleon	soft	3.8	1.5				0.09	0.10
Ne + Cu	exp.	8.6	3.1	0.66	0.44		0.14	
400 MeV/nucleon	soft	8.8	4.0				0.17	0.20
C + C	exp.	2.2	0.41	0.039	0.034			0.16
800 MeV/nucleon	soft	2.2	0.54				0.18	0.18
Ne + NaF	exp.	5.1	1.12	0.16	0.14		0.36	0.41
800 MeV/nucleon	soft	5.2	1.46				0.42	0.42
Ar + KCl	exp.	14.1	4.0	0.62	0.52	0.16	1.0	1.4
800 MeV/nucleon	soft	13.3	4.60				1.11	1.47
	stiff	13.5	4.55				1.00	1.32
Ar + Pb	exp.	43.0	18.9	5.0	2.7	1.4	2.2	4.3
800 MeV/nucleon	soft	47.0	19.7				3.4	6.9
	stiff	46.7	20.5				2.8	6.2
Na + NaF	exp.	5.1	0.8	~ 0.07	~ 0.05		~ 1.6	1.63
2100 MeV/nucleon	soft	5.8	0.9				1.40	1.50

The 100 MeV/nucleon data are from ref. ³⁸⁾ and the remaining data are from ref. ¹⁾. The uncertainties in the measured yields from the 100 MeV/nucleon reaction are: 2% for p, 3% for d and ^3H , 6% for ^3He , and 10% for ^4He . The uncertainties in absolute values of yields from ref. ¹⁾ are: 20% for p and d, and 30% for ^3H , ^3He , π^+ and π^- . However, uncertainties in relative yields are smaller, in particular 10% for d to p and 20% for π^- to p. The symbol “ \sim ” in front of a figure indicates uncertainty of 40–50%. The calculations are for the soft and stiff equations of state.

parameter f_c in eq. (2.28). With less restrictive cut-offs than we have used, the number of low-momentum deuterons in the calculation increases. The data by Nagamiya *et al.* ¹⁾ have been taken at large angles, outside of the fragmentation regions, and extrapolated to small angles and low energies. We compare their numbers with ours following a similar procedure, taking the yields for sideways directions only and extrapolating to the full 4π solid angle. At 100 MeV/nucleon we overestimate the proton and deuteron yields, but the ratio of calculated yields is close to the ratio of experimental yields. At this energy a substantial number of nucleons is emitted in other light fragments. At higher energies we reproduce the experimental proton yields. We typically overestimate somewhat the deuteron yields. The deuteron-to-proton (d/p) ratio changes by less than 5% when the mean-field parameters are changed. The mass dependence of the d/p ratio in reactions at 800 MeV/nucleon is illustrated in fig. 8. The calculated pion yields are consistent

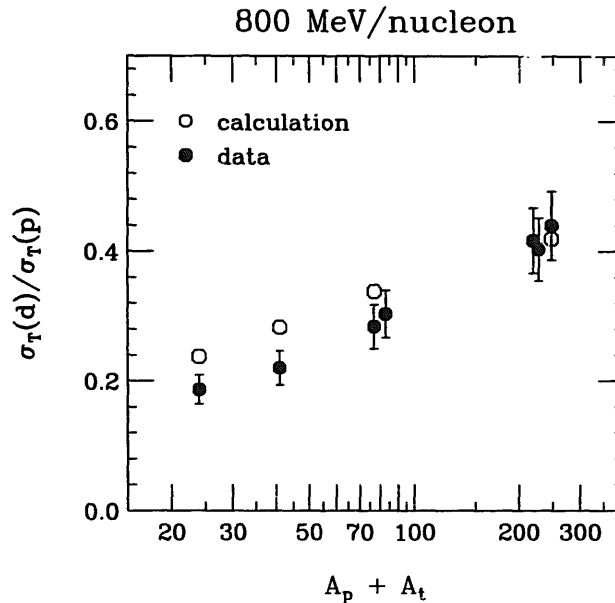


Fig. 8. Ratio of deuteron-to-proton yields in the 800 MeV/nucleon reactions as a function of the sum of projectile and target masses.

with the experimental yields, except for the case of Ar+Pb at 800 MeV/nucleon. The values of calculated and experimental π^+ -to- π^- ratios in the systems with significant isospin asymmetry are consistent with values of $(Z/N)^2$ in the participant region¹⁾. In the calculation, the deuteron formation reduces somewhat N_p/N_n compared to Z/N , cf. eq. (4.9).

We next compare the calculated spectra of particles with data in figs. 9–11. At 100 MeV/nucleon we obtain too many particles emitted with intermediate momenta compared to the data, and too few particles emitted with very forward momenta. This can be related to the use of free-scattering cross sections in the calculations. Except for 10° in Ar+KCl system, the description of proton spectra in the reactions at 800 MeV/nucleon is quite remarkable. In the deuteron spectra we have problems with the fragmentation peak, figs. 10b and 11b. There are too few negative pions produced at low momenta in the forward direction compared to the data. The description of the 800 MeV/nucleon data is, otherwise, fair.

We turn to comparison of our results with the multiplicity-selected data. The ratios of composite to proton yields have been studied as functions of participant baryon charge multiplicity by the Plastic Ball Group^{77,78)}. The experimentalists have identified the different particles and established the ratios in a portion of the full momentum space. In fig. 12 we compare our results for d/p ratio at wide angles with the data^{77,78)} from Nb+Nb reaction at 650 MeV/nucleon. The baryon charge multiplicity in the calculation is determined using the same cuts as in the experiment⁷⁸⁾. In this and other systems we reproduce the rise of the ratio with increasing centrality of the collision. However, the overall magnitudes are not always as well reproduced as in the case in fig. 12. In particular, the energy dependence of the

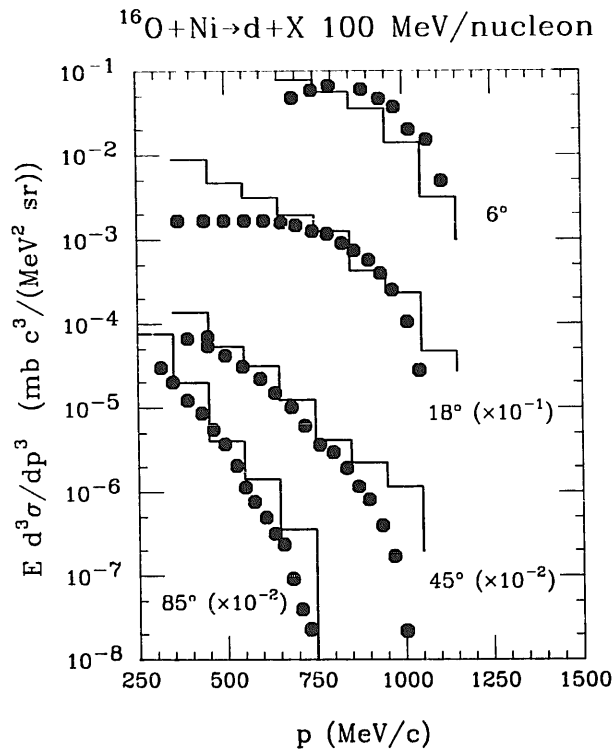
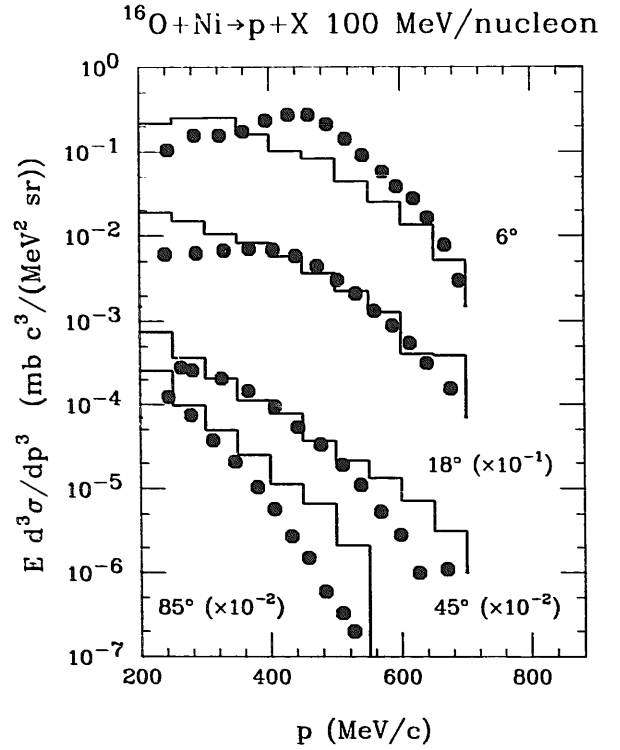


Fig. 9. Proton and deuteron spectra from 100 MeV/nucleon $^{16}\text{O} + \text{Ni}$ reaction. Data from ref. ³⁸⁾ are indicated with dots and the results of calculation with histograms.

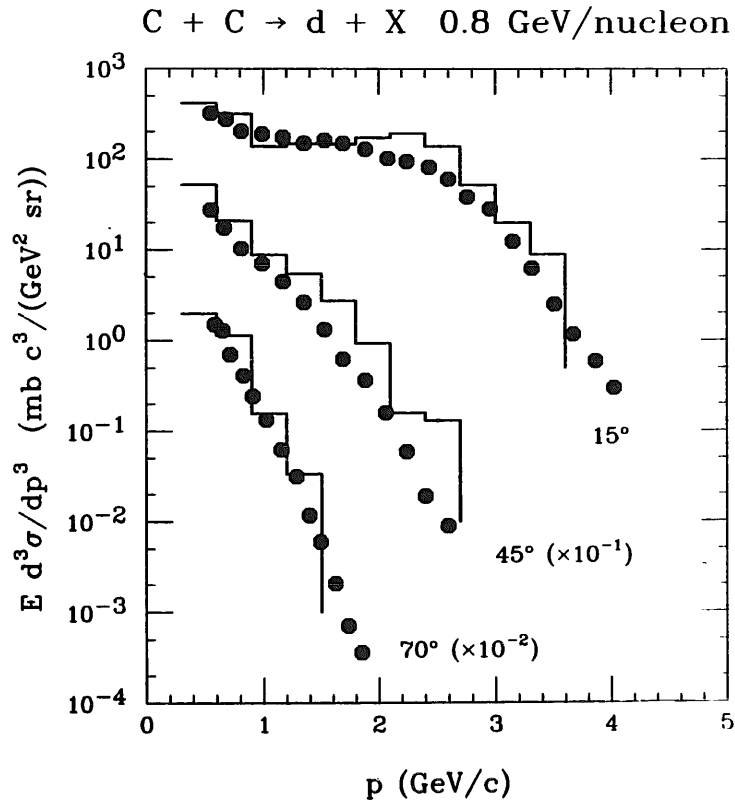
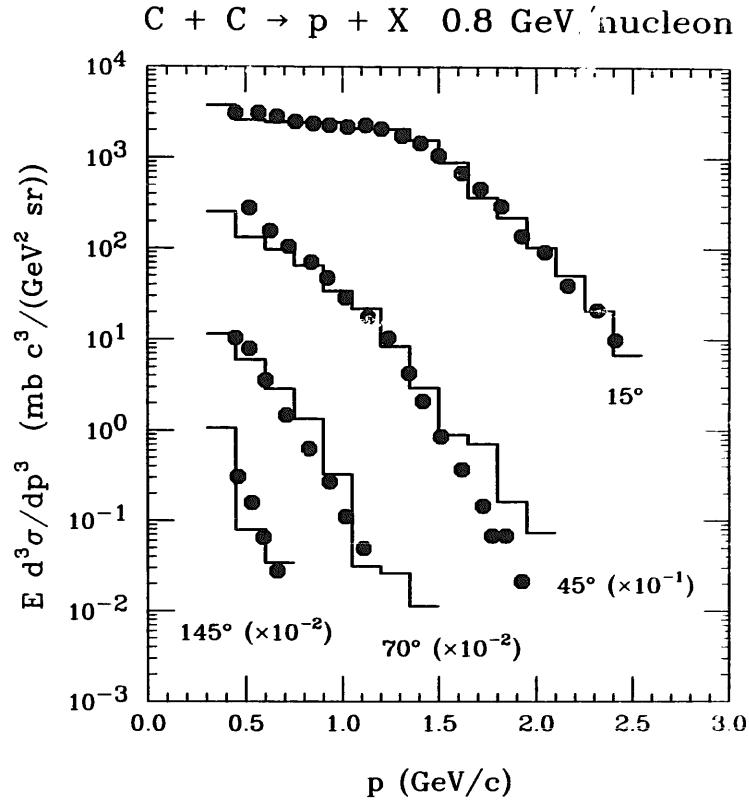


Fig. 10. Proton, deuteron and negative-pion spectra from 800 MeV/nucleon $^{12}\text{C} + ^{12}\text{C}$ reaction. Data from ref. ¹⁾ are indicated with dots and the results of calculation with histograms.

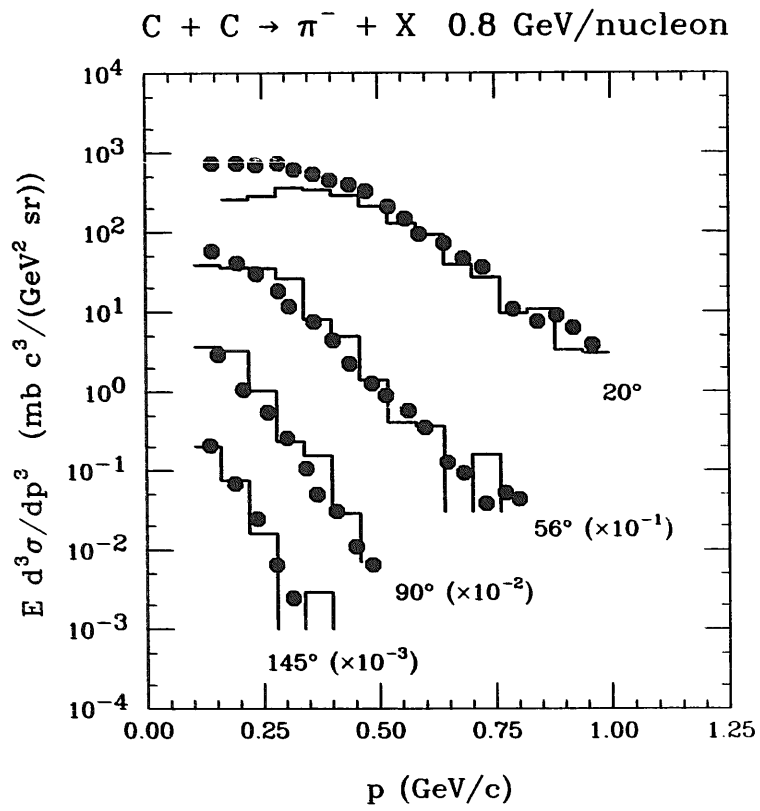


Fig. 10—continued

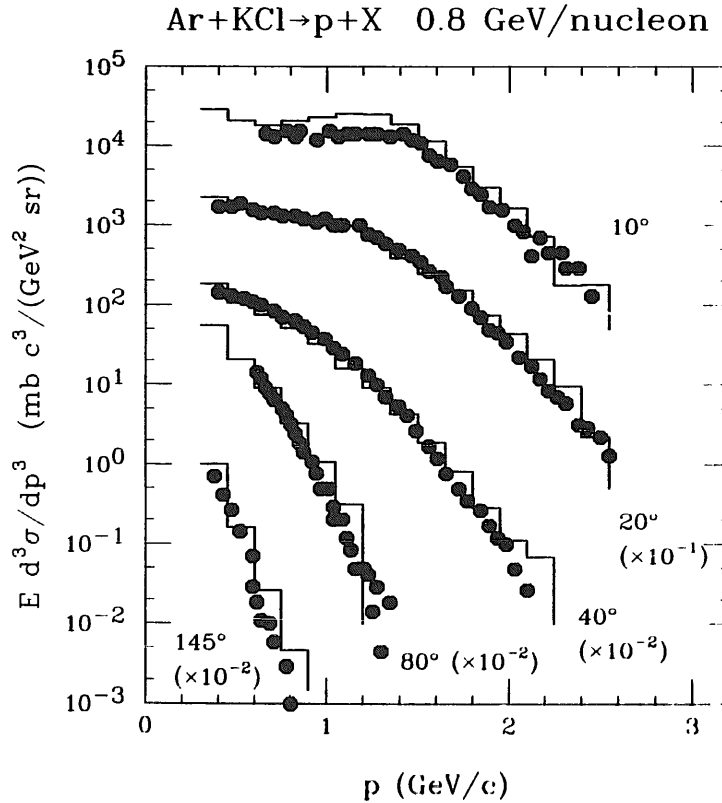


Fig. 11. Proton, deuteron and negative-pion spectra from 800 MeV/nucleon Ar+KCl reaction. Data from ref. 1) are indicated with dots and the results of calculation with histograms.

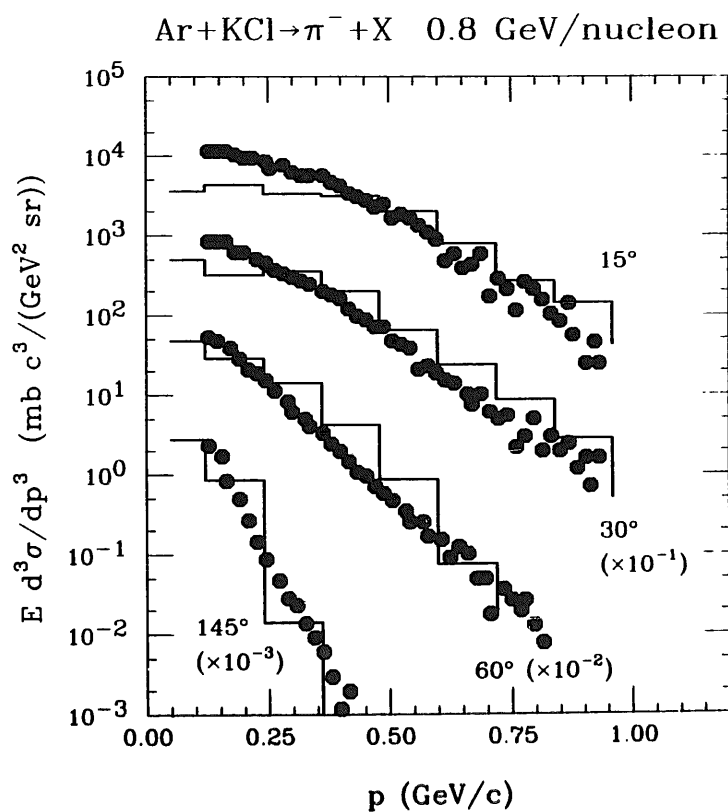
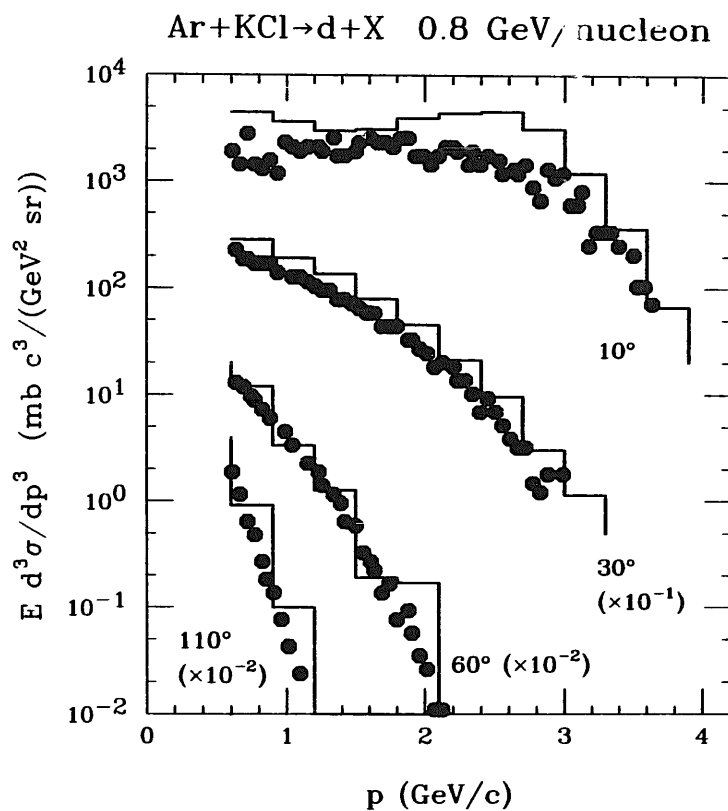


Fig 11—continued

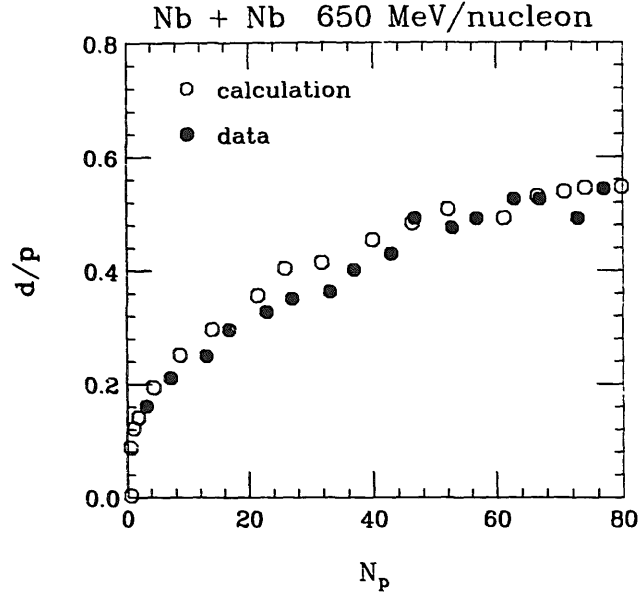


Fig. 12. Ratio of deuteron-to-proton yields at wide angles as a function of participant proton multiplicity in the 650 MeV/nucleon Nb + Nb reaction. Data from refs. ^{77,78)} are indicated with filled circles and the results of calculations with open circles.

calculated d/p ratio is stronger for high multiplicity than observed. Experimentally, the ratios of other composites to protons exhibit stronger energy dependence than the ratio of deuterons to protons ⁷⁸⁾. Changing from the soft to stiff equation of state results in a $\sim 4\%$ rise of the ratio for the $b = 0$ case of fig. 12. Similar sensitivity to the equation of state is found for other bombarding energies. We essentially confirm the result of ref. ¹³⁾ and contradict that of ref. ³¹⁾.

The d/p ratio has been proposed as a measure of the entropy produced in reactions by Siemens and Kapusta ⁷⁹⁾, cf. also refs. ^{9,13,80-84)}. The entropy is expressed in terms of particle distributions as

$$S = - \sum_{\tau} \frac{g_{\tau}}{(2\pi)^3} \int d\mathbf{r} \int d\mathbf{p} (f_{\tau} \log f_{\tau} \pm (1 \mp f_{\tau}) \log (1 \mp f_{\tau})), \quad (6.1)$$

where upper signs refer to fermions and lower to bosons. In the limit of Boltzmann statistics, the entropy of an equilibrated system of nucleons and deuterons can be expressed in terms of the d/p ratio:

$$\frac{S}{A} = \frac{5}{2} \frac{1+r-r\zeta}{1+r} - \log \frac{r}{3\sqrt{2}} - \zeta \log \frac{\zeta}{1-\zeta+r(1-2\zeta)}, \quad (6.2)$$

where $r = N_p/N_d$, and $\zeta = Z/A$. For $\zeta \approx \frac{1}{2}$, the expression simplifies to ⁴³⁾

$$\frac{S}{A} = \frac{5}{4} \frac{2+r}{1+r} - \log \frac{r}{3\sqrt{2}}. \quad (6.3)$$

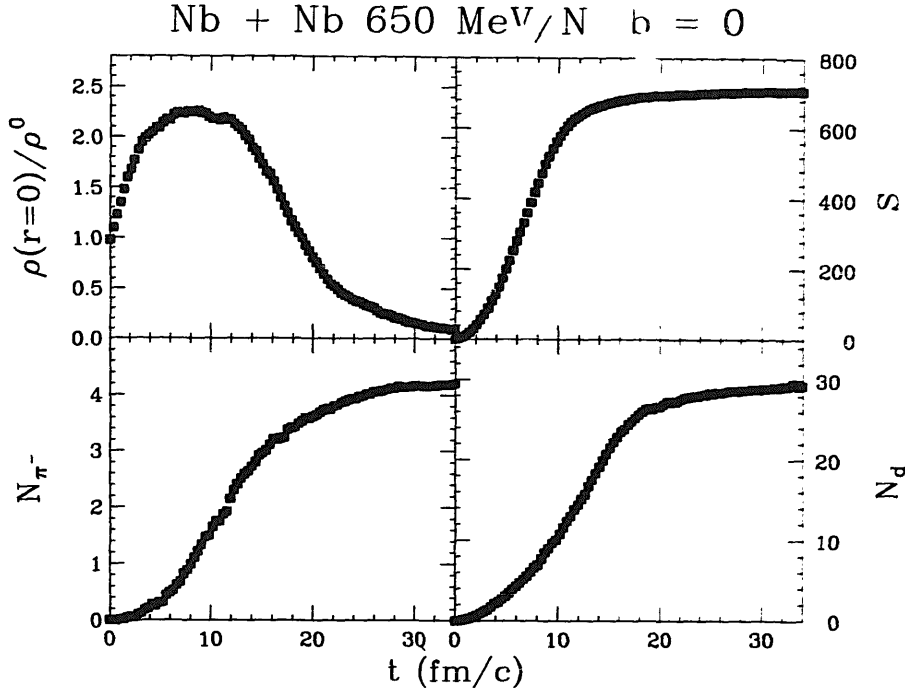


Fig. 13. Evolution of the central baryon density, total entropy, negative-pion number, and deuteron number in a central Nb+Nb collision at 650 MeV/nucleon, for the stiff equation of state.

In fig. 13 we show the variation of deuteron number and entropy with time in the central Nb+Nb collision at 650 MeV/nucleon, together with the variation of spatial density and pion number. In fig. 14 we show the entropy per baryon obtained from (6.1) for different impact parameters, for nucleons and deuterons emitted at wide angles, and compare it to the estimate from (6.2). The results agree at 650 MeV/nucleon for the intermediate and low intermediate impact parameters, to within ~ 0.25 . We believe that we can determine S in eq. (6.1) with an accuracy of ~ 0.1 per nucleon. For lower bombarding energies shown in fig. 15, the discrepancy between the results from (6.1) and (6.2) grows.

In figs. 14 and 15 we show the values of entropy extracted from the data using the quantum statistical model (QSM) [refs. ^{78,84,83}]. Although our d/p ratios agree with the data taken at 650 MeV/nucleon, we obtain higher values of entropy than extracted using the QSM model with a difference of 0.5 or more per nucleon for central collisions and the soft equation of state. This is due to inclusion of heavier composites in the QSM data analysis; in essence, the entropy per nucleon for a composite with mass A is lower by the amount of $\frac{5}{2}(A-1)/A$ than the nucleon entropy under the conditions of equilibrium. The entropies extracted from the QSM fit and the naive d/p ratio are then necessarily different. We can see within our model the effect of composites on the entropy production by suppressing the formation of deuterons in the calculation. Without deuteron production we obtain the entropy per nucleon lower by ~ 0.15 . We can then expect that if the production of heavier composites occurred in the calculation, then the discrepancy between

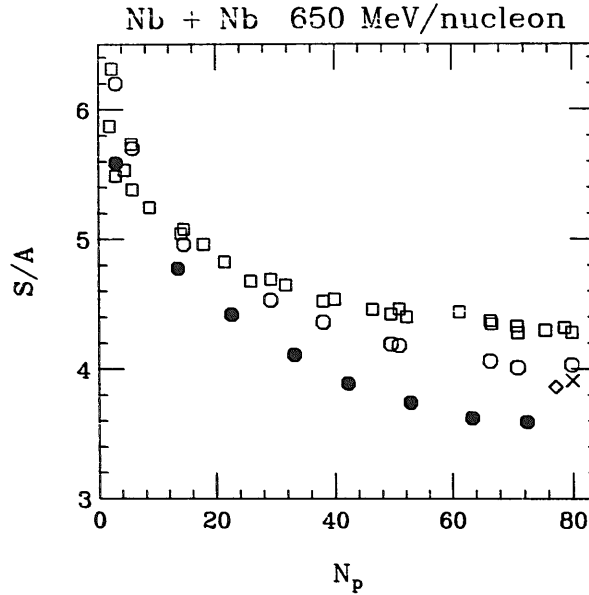


Fig. 14. Entropy per nucleon produced in Nb+Nb collisions at 650 MeV/nucleon as a function of participant proton multiplicity. Open circles and squares indicate, respectively, the results from eqs. (6.1) and (6.2) obtained using the soft equation of state. Cross indicates a $b=0$ result from (6.1) for the stiff equation of state. Diamond indicates a $b=0$ result obtained without deuteron production and using soft equation of state. Filled circles indicate the entropy extracted from the data in ref. ⁷⁸) using QSM model of ref. ⁸⁴).

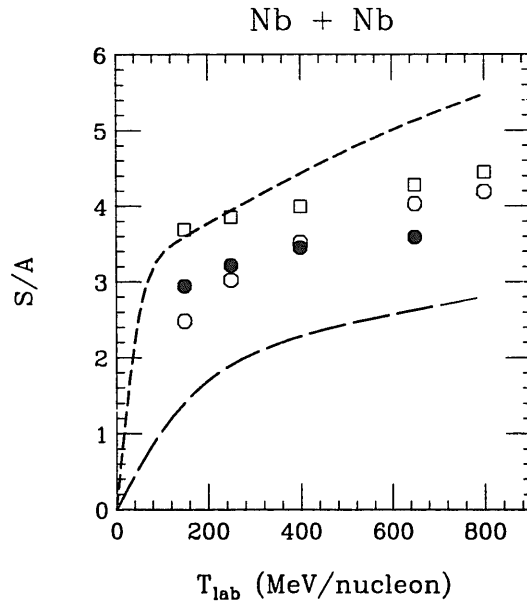


Fig. 15. Entropy per nucleon produced in central Nb + Nb collisions as function of bombarding energy. Open circles and squares indicate, respectively, the results from eqs. (6.1) and (6.2), using soft equation of state. Filled circles indicate the entropy extracted from the data in ref. ⁷⁸) using the QSM model. The short-dashed and long-dashed lines indicate, respectively, the results from the fireball and hydrodynamical models, given in ref. ⁷⁸).

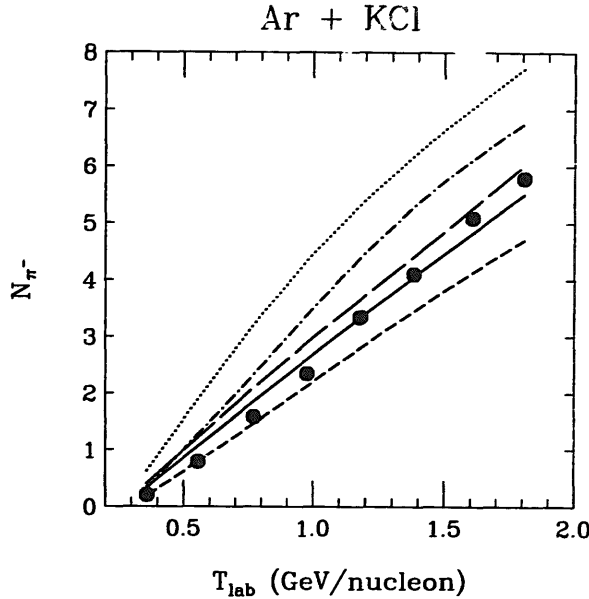


Fig. 16. Negative-pion multiplicity as a function of the bombarding energy per nucleon in central Ar + KCl collisions. Dots indicate data of ref. ¹⁹). Calculations were done for $b = 1.7$ fm. The long-dashed and solid line indicate the results for the soft and stiff equation of state, respectively. The short-dashed line is obtained in the frozen resonance approximation. The dash-dotted line indicates the results obtained following our procedures in the cascade-model limit, i.e. without optical potential, Pauli principle, and deuteron production. The dotted line indicates the results obtained in the cascade-model limit following the procedures in the literature, using eq. (4.1) and sampling the resonance masses from respective spectral functions (4.3).

the calculated entropy and that extracted from data at 650 MeV/nucleon would grow. The change from a soft to stiff equation of state decreases the discrepancy by only 0.1. We also note that the entropy calculated in our model using (6.2) may be too high compared to (6.1) due to the deuteron cutoff condition, eq. (2.28). The QSM analysis ^{78,84}) was made with an excluded volume condition which plays a similar role to our deuteron cutoff (2.28). Since the entropy is expected to tend to zero with decreasing bombarding energy, the ratios of composites to protons for given entropy may be overestimated in the particular form of the QSM model ⁸⁴) used to analyze the data ⁷⁸), for lower bombarding energies.

In fig. 16 we compare the results of our calculations with the multiplicity of negative pions produced in central Ar + KCl collisions ¹⁹). The data from the streamer chamber group has been the subject of much previous theoretical study. The long-dashed and solid lines correspond, respectively, to the soft and stiff equation of state. Clearly, the pion yield is not sensitive enough to the equation of state to use such data to distinguish different models. The short-dashed line is computed with the frozen resonance approximation, i.e. not allowing the deltas to decay during the course of the heavy-ion collision. This evidently allows more reabsorption and lowers the final pion yield. The dotted and dash-dotted lines are computed in the

cascade-model limit, i.e. with the mean field turned off. These curves illustrate the importance of the detailed balance condition: the dotted line is obtained following earlier treatments^{25,17)} of the resonance production and absorption using the relation (4.1), and the dot-dashed line is obtained using the (4.16). The difference between the lines comes entirely from a difference in the number of resonances reabsorbed in interactions with nucleons. Thus a substantial portion of the discrepancy between the cascade-model results and the data may be attributed to the improper detailed balance relation. For a system heavier than Ar+KCl, the reabsorption would be even more important and the effect of the different balance relations would be more dramatic. When the reabsorption cross sections from (4.1) and frozen delta approximation are combined, results close to the data may be obtained³⁰⁾. With (4.16) we get results that are close but at a high side of the data for lower energies, cf. fig. 15 and table 1. If deuteron quasiparticles were permitted to participate in pion production, the calculated yields would be somewhat higher. We note also that there may be some sensitivity to the momentum dependence of the mean field. This was shown to reduce the predicted rate for producing pions³⁰⁾.

7. Discussion

We have derived a transport equation for two-body bound states with production and absorption terms for the bound states. Two-body bound states are produced in three-body collisions in the process that is inverse to the bound-state breakup. We describe the elementary features of few-body collisions. A formal expansion of production and absorption rates in terms of the number of interacting quasiparticles is given in ref.⁴²⁾. A sequence of two-body processes contributes to three- or more-body collision, when kinematic restrictions are such that particles cannot appear on shell in between the processes.

In parametrizing the matrix element for deuteron formation, we apply the impulse approximation and renormalize the matrix element so that measured cross sections for deuteron breakup are reproduced.

We find that the usual approach^{16,17,25-34)} to pion production, via the formation and decay of variable-mass resonances, may be derived microscopically, provided the decay rate is large compared to time variation of the resonance production rate. We show that detailed balance relation used in the literature to obtain the delta reabsorption cross section is not valid for short-lived particles. In the cascade model and in models based on same assumptions, the relation leads to equilibrium with a greater number of pions than in the fireball model.

In solving the set of transport equations for the energetic heavy-ion collisions, we find that we can largely reproduce the measured particle yields and spectra. The calculated relative deuteron yield increases with the mass of the system and the

centrality of the collision. At 650 MeV/nucleon we exceed by ~ 0.5 the entropy per nucleon in the calculation compared to the entropy extracted from the measured composite yields. Neither the deuteron yield nor entropy exhibit a sensitivity to the equation of state at a detectable level.

The pion yields differ by 10–15% depending on the equation of state, but this is not strong enough to tell the stiff and soft equations apart in practice. Concerning our result on the relation between the delta production and absorption cross section it might be interesting to see whether use of the correct detailed balance would reduce the disagreement²⁷⁾ between the cascade predictions and the data for pion–nucleus and proton–nucleus interactions.

For reasons stated at the end of sect. 4, we do not consider by any means the issue of the mechanism for pion production closed. We intend to investigate the question of production with the delta resonance appearing only as a virtual particle. Concerning the deuteron production, a weakness of the current model is that the deuteron formation time is somewhat long (or size large). We intend to evolve⁸⁵⁾ the model in such a manner that reliance on the shortness of the formation time disappears, and the model is extended to include the production of other light composites.

The authors acknowledge the discussions with W. Bauer, B.-A. Li, D. Brink, H.S. Kohler, F. Osterfeld, E.A. Remler, and P. Schuck. One of the authors (P.D.) has benefited from a collaboration with B. Chen. The authors thank A. Poskanzer for providing them with a plastic ball filter program. Some of the calculations for the paper have been carried out using computing facilities of the Institute for Nuclear Theory at Seattle. This work was supported by the National Science Foundation under Grant Nos. PHY-8905933 and PHY-9017077.

Appendix

NUMERICAL METHOD

We represent the distribution functions f_N, f_d, f_π and $\ell_r A_r$, with sets of pseudoparticles. The resonance distribution, $\ell_r A_r$, is, up to a factor, a density in space, momentum and mass, while other functions are densities in space and momentum. The representations at any time instant are

$$\frac{g}{(2\pi)^3} f \approx \frac{1}{\mathcal{N}} \sum_k \delta(\mathbf{R} - \mathbf{R}_k) \delta(\mathbf{p} - \mathbf{p}_k), \quad (\text{A.1})$$

$$\frac{g}{(2\pi)^4} \ell A \approx \frac{1}{\mathcal{N}} \sum_k \delta(\Delta m_k) \delta(\mathbf{R} - \mathbf{R}_k) \delta(\mathbf{p} - \mathbf{p}_k), \quad (\text{A.2})$$

where \mathcal{N} is a number of pseudoparticles per particle. The pseudoparticle positions

and momenta are taken to satisfy

$$d\mathbf{R}_k/dt = \partial e_k / \partial \mathbf{p}_k, \quad (\text{A.3})$$

$$d\mathbf{p}_k/dt = -\partial e_k / \partial \mathbf{R}_k. \quad (\text{A.4})$$

This serves to integrate the drift terms in the equations for the distribution functions, such as at the l.h.s. of eqs. (3.5) and (4.10). Times for evaluating positions and momenta are shifted by half of a time step, $\frac{1}{2}\Delta t$, in order to make this integration approximately of second order in time^{17,86}).

For the purpose of evaluating the optical potential and the collision integrals, the calculational volume is divided into cells of volume $\Delta V = (\Delta l)^3$. After each time when the pseudoparticles are moved in space, they are sorted according to their cell location. Pointers are set up so that all pseudoparticles in any cell are immediately accessible.

For any two pseudoparticles in one cell the interaction cross section σ is evaluated with the probability $\mathcal{N}_c/\mathcal{N}$, $\mathcal{N}_c \leq \mathcal{N}$. In the case of the nucleon pseudoparticles, the volume \mathcal{V} , eq. (3.20), is evaluated for other nucleon pseudoparticles in a cell, that can lead to deuteron formation, with the probability $\mathcal{N}_c/\mathcal{N}$. The three-body collision is further processed with the probability

$$\sigma_{12}v_{12}\mathcal{V}_3\Delta t/(\mathcal{N}_c\Delta V)^2, \quad (\text{A.5})$$

where 1 and 2 are neutron and proton, and twice as large otherwise. The cosine of a c.m. angle between the deuteron momentum and the momentum of a spectator nucleon 3 is sampled according to

$$|\langle \tilde{p}_3 | \phi \rangle|^2, \quad (\text{A.6})$$

cf. eq. (3.20). This is done by having an integral such as at the r.h.s. of the equality in (3.20) tabulated, and using an inverse method with section strategy to obtain the cosine. The probability density for deuteron formation is uniform, in our model, in the azimuthal angle about the momentum of a spectator nucleon. The collision occurs, if the condition (2.28) is satisfied, with a probability $(1-f)$ associated with the nucleon in the final state. We ignore the deuteron statistics of which the effect would be small under the condition (2.28), as $f_d \sim f^2$ for the same momentum per nucleon.

If the selected pseudoparticles are not involved in a three-body collision, a two-body collision is processed with the probability

$$\sigma v \Delta t / (\mathcal{N}_c \Delta V). \quad (\text{A.7})$$

In the case of deuteron breakup, the c.m. momentum of a spectator nucleon p_3^* is sampled according to the subintegral function in (3.15). This is done by mapping the interval from 0 to $p_3^{*\max}$ onto 0 to 1, and applying the Metropolis algorithm. The drawing in each case extends over the whole interval, and the value of p_3^* is picked after $N_{\mathcal{D}}$ drawings. We have used $N_{\mathcal{D}} = 10-20$. The value in the interval

from 0 to 1 is retained as a starting value for the next breakup. After the value of p_3^* is picked up, a statistical decision is made on the identity of the spectator and participant nucleons, according to the values of NN cross sections, eq. (3.15). Next, the cosine of a c.m. angle between the deuteron momentum and that of a spectator nucleon is sampled according to (A.6). The breakup cross section is uniform in our model in the azimuthal angle of a spectator nucleon with respect to the deuteron, and in the spherical angle of the participating nucleons in their c.m.

For the $2 \rightarrow 2$ processes with nucleons and deltas, the inversion for the scattering angle can be done analytically when using the cross sections from refs. ^{17,33}). Rather than the mass, eq. (4.13), in case of a resonance in the final state, we sample the c.m. momentum,

$$m \, dm = \frac{\mathcal{E}^* + e'^*}{e'^*} p'^* \, dp'^* . \quad (\text{A.8})$$

The sampling is done using the Metropolis algorithm as in the case of deuterons.

For the purpose of evaluating the Pauli-blocking factors, a smooth distribution f is extracted from the distribution of pseudoparticles using a parametric form

$$f = \frac{\mathcal{A}'}{\exp((\sqrt{m^2 + \tilde{p}^{\prime 2}} - \mu')/T') + 1)} + \frac{\mathcal{A}''}{\exp((\sqrt{m^2 + \tilde{p}^{\prime\prime 2}} - \mu'')/T'') + 1)} . \quad (\text{A.9})$$

Here the two terms correspond, respectively, to the pseudoparticles from projectile and target nuclei. This parametrization is flexible enough to describe the distributions in both the initial stage of the reaction and in a fully equilibrated final state. The parameters for the distribution are established from the pseudoparticles in a given cell and the neighboring cells, in a sequence of steps. First, the rest frames for the particles from projectile and target are determined. Next, for the two groups of particles the moments

$$c^{ij} = \langle p^i p^j \rangle \quad (\text{A.10})$$

are evaluated in the respective frames. The momenta are then rescaled to define the \tilde{p}^2 which appear in (A.9). This is given by

$$\tilde{p}^2 = \sum_{i,j} \beta_{ij} p^i p^j , \quad (\text{A.11})$$

where

$$\beta_{ij} = \frac{1}{3} (c^{-1})_{ij} \langle p^2 \rangle , \quad (\text{A.12})$$

However, if the principal axes of the momentum tensor do not differ by enough to be statistically significant, the rescaling is suppressed or is the same for two of the directions. The average momentum squared is $\langle p^2 \rangle = \text{Tr}(c) = \langle \tilde{p}^2 \rangle$. For the two groups of particles values of $\langle |\tilde{p}| \rangle$ in the respective frames are calculated. Finally for the given $\langle |\tilde{p}| \rangle$, and $\langle \tilde{p}^2 \rangle$, tabulated values are used to obtain $\mu - m$, and T . In cases $\langle \tilde{p}^2 \rangle$

falls below the minimum compatible with a given $\langle |\tilde{p}| \rangle$, it is reset to the minimum value. The constants \mathcal{A} in (A.9) are determined from the invariant density $\tilde{\rho}_s$, corresponding to given $\mu - m$ and T

$$\mathcal{A} = \frac{(\frac{1}{3}\langle p^2 \rangle)^{3/2}}{(\det(c))^{1/2}} \frac{\rho_s}{\tilde{\rho}_s}. \quad (\text{A.13})$$

The invariant densities are used separately for the two groups of particles. Finally, if f at the center of one of the distributions is found to exceed 1, then the $\langle |\tilde{p}| \rangle$ for that distribution is increased until the f is reduced to 1. The neutron and proton pseudoparticles were grouped jointly in most cases.

In calculating the entropy we use (A.9) and the fact that the entropy changes only due to collisions and decays, and we reevaluate the entropy only in the cells where collisions or decays occur. The calculation of the deuteron entropy is problematic because the number statistics is low. We therefore made the approximation $f_d = f_p f_n$ in the argument of the logarithm. Here the nucleon distributions are taken at half the deuteron momentum in the frame of the distribution. We also tried other procedures to get the deuteron entropy, obtaining similar results. In any case, the additional entropy coming from the production of deuterons is small.

The values of the parameters in the calculations are: $\mathcal{N} = 60\text{--}600$, with $\mathcal{N} = 170$ used most often, $\mathcal{N}_c = 40$, $\Delta l = 0.9$ fm, and $\Delta t = 0.15\text{--}0.35$ fm/ c . Stability of the results with respect to the variation in all of these parameters has been tested. The colliding systems were further enclosed into a box, the optical potential was put equal to zero, and the Pauli principle was temporarily switched off, to verify whether the equilibrium numbers of pions and deuterons and the equilibrium value of entropy were obtained after prolonged evolution.

References

- 1) S. Nagamiya, M.-C. Lemaire, E. Moeller, S. Schnetzer, G. Shapiro, H. Steiner and I. Tanihata, *Phys. Rev. C* **24** (1981) 971
- 2) J. Gosset, J.I. Kapusta and G.D. Westfall, *Phys. Rev. C* **18** (1978) 844
- 3) A.Z. Mekijan, *Phys. Rev. C* **17** (1978) 1051; *Nucl. Phys. A* **312** (1978) 491
- 4) J. Kapusta, *Phys. Rev. C* **21** (1980) 1301
- 5) S. DasGupta and A.Z. Mekijan, *Phys. Reports* **72** (1981) 971
- 6) H.H. Gutbrod, A. Sandoval, P.J. Johansen, A.M. Poskanzer, J. Gosset, W.G. Meyer and G.D. Westfall, *Phys. Rev. Lett.* **C21** (1976) 667
- 7) J. Gosset, H.H. Gutbrod, W.G. Meyer, A.M. Poskanzer, A. Sandoval, R. Stock and G.D. Westfall, *Phys. Rev. C* **16** (1977) 629
- 8) M.-C. Lemaire, S. Nagamiya, S. Schnetzer, H. Steiner and I. Tanihata, *Phys. Lett. B* **85** (1979) 38
- 9) G. Bertsch and J. Cugnon, *Phys. Rev. C* **24** (1981) 2514
- 10) H. Sato and K. Yazaki, *Phys. Lett. B* **98** (1981) 153
- 11) E.A. Remler, *Ann. of Phys.* **136** (1981) 293; *Phys. Rev. C* **25** (1982) 2974
- 12) M. Gyulassy, K. Frankel and E.A. Remler, *Nucl. Phys. A* **402** (1983) 596
- 13) J. Aichelin and E.A. Remler, *Phys. Rev. C* **35** (1987) 1291
- 14) Y. Yariv and Z. Fraenkel, *Phys. Rev. C* **20** (1979) 2227
- 15) J. Cugnon, *Phys. Rev. C* **22** (1980) 1885
- 16) G.F. Bertsch, S. DasGupta and H. Kruse, *Phys. Rev. C* **29** (1984) 673

- 17) G.F. Bertsch and S. DasGupta, *Phys. Reports* **160** (1988) 189
- 18) P. Danielewicz, *Ann. of Phys.* **152** (1984) 239, 305
- 19) A. Sandoval, R. Stock, H.E. Stelzer, R.E. Renfordt, J.W. Harris, J.P. Brannigan, J.V. Geaga, L.J. Rosenberg, L.S. Schroeder and K.L. Wolf, *Phys. Rev. Lett.* **45** (1980) 874
- 20) R. Stock, R. Bock, J.W. Harris, A. Sandoval, H. Stroebele, K.L. Wolf, H.G. Pugh, L.S. Schroeder, M. Maier, R.E. Renfordt, A. Dacal and M.E. Ortiz, *Phys. Rev. Lett.* **49** (1982) 1236
- 21) R. Stock, *Phys. Reports* **135** (1986) 259
- 22) M. Sano, M. Gyulassy, M. Wakai and Y. Kitazoe, *Phys. Lett.* **B156** (1985) 27
- 23) J.I. Kapusta, *Phys. Rev.* **C16** (1977) 1493
- 24) J. Cugnon, T. Mizutani and J. Vandermeulen, *Nucl. Phys.* **A352** (1981) 505
- 25) J. Cugnon, D. Kinet and J. Vandermeulen, *Nucl. Phys.* **A379** (1982) 553
- 26) M. Cahay, J. Cugnon and J. Vandermeulen, *Nucl. Phys.* **A411** (1983) 524
- 27) J. Cugnon and M.-C. Lemaire, *Nucl. Phys.* **A489** (1988) 781
- 28) H. Kruse, B.V. Jacak and H. Stöcker, *Phys. Rev. Lett.* **54** (1985) 289
- 29) Y. Kitazoe, M. Sano, H. Toki and S. Nagamiya, *Phys. Lett.* **B166** (1986) 35
- 30) C. Gale, *Phys. Rev.* **C36** (1987) 2152
- 31) J. Aichelin, A. Rosenhauser, G. Peilert, H. Stöcker and W. Greiner, *Phys. Rev. Lett.* **58** (1987) 1926
- 32) J.J. Molitoris, H. Stöcker and B.L. Winer, *Phys. Rev.* **C36** (1987) 220
- 33) Gy. Wolf, G. Batko, W. Cassing, U. Mosel, K. Niita and M. Schäfer, *Nucl. Phys.* **A517** (1990) 615
- 34) B.-A. Li and W. Bauer, *Phys. Lett.* **B254** (1991) 335; Pion spectra in a hadronic transport model for relativistic heavy-ion collisions, report MSUCL-759 (1991)
- 35) R. Stock, R. Bock, R. Brockmann, A. Dacal, J.W. Harris, M. Maier, M.E. Ortiz, H.G. Pugh, R.E. Renfordt, A. Sandoval, L.S. Schroeder, H. Stroebele and K.L. Wolf, *Phys. Scr.* **T5** (1983) 130
- 36) J.W. Harris and R. Stock, *Notas de Fisica* **7** (1984) 61
- 37) J.W. Harris, R. Bock, R. Brockmann, A. Sandoval, R. Stock, H. Stroebele, G. Odyniec, H.G. Pugh, L.S. Schroeder, R.E. Renfordt, D. Schall, D. Bangert, W. Rauch and K.L. Wolf, *Phys. Lett.* **B153** (1985) 377
- 38) R.L. Auble, J.B. Ball, F.E. Gertrand, C.B. Fulmer, D.C. Hensley, I.Y. Lee, R.L. Robinson, P.H. Stelson, C.Y. Wong, D.L. Hendrie, H.D. Holmgren and J.D. Silk, *Phys. Rev.* **C28** (1983) 1552
- 39) W. Botermans and R. Malfliet, *Phys. Reports* **198** (1990) 115
- 40) D.F. DuBois, in *Lectures in theoretical physics*, ed. W.E. Brittin, vol. IXC (Gordon and Breach, New York, 1967) p. 469
- 41) L.P. Kadanoff and G. Baym, *Quantum statistical mechanics* (Benjamin, New York, 1962)
- 42) P. Danielewicz, *Ann. of Phys.* **197** (1990) 154
- 43) L.P. Csernai and J.I. Kapusta, *Phys. Reports* **131** (1986) 223
- 44) R.F. Bishop, M. Strayer and J.M. Irvine, *Phys. Rev.* **A10** (1974) 2423; *J. Low Temp. Phys.* **20** (1975) 573;
H.B. Ghasib, R.F. Bishop and M.R. Strayer, *J. Low. Temp. Phys.* **23** (1976) 393
- 45) G. Röpke, L. Münchow and H. Schulz, *Nucl. Phys.* **A379** (1982) 536; *Phys. Lett.* **B110** (1982) 21;
G. Röpke, M. Schlanges, D. Kremp, L. Münchow and H. Schulz, *Yad. Fiz.* **36** (1982) 607
- 46) B.E. Vonderfecht, C.C. Gearht, W.H. Dickhoff, A. Polls and A. Ramos, *Phys. Lett.* **B253** (1991) 1
- 47) P. Danielewicz, *Phys. Rev.* **C42** (1990) 1564
- 48) G. Röpke and H. Schulz, *Nucl. Phys.* **A477** (1988) 472
- 49) A.I. Akhiezer and S.V. Peletminski, *Metody statisticheskoy fiziki* (Nauka, Moscow, 1977)
- 50) J.A. McLennan, *Introduction to nonequilibrium statistical mechanics* (Prentice-Hall, Englewood Cliffs, 1989)
- 51) M.L. Goldberger and K.M. Watson, *Collision theory* (Wiley, New York, 1964)
- 52) P. Danielewicz and P. Schuck, submitted to *Nucl. Phys. A*
- 53) S. Mrówczyński and P. Danielewicz, *Nucl. Phys.* **B342** (1990) 345
- 54) B. Bezzerides and D.F. DuBois, *Ann. of Phys.* **70** (1972) 10
- 55) W. Botermans and R. Malfliet, *Phys. Lett.* **B215** (1988) 617
- 56) I. Lovas, *Nucl. Phys.* **A343** (1980) 435
- 57) J.D. Seagrave, in: *Three-body problem in nuclear and particle physics*, ed. J.S.C. McKee and P.M. Rolph (North-Holland, Amsterdam, 1970) p. 41

- 58) R.F. Carlson *et al.*, in: Few-particle problems in the nuclear interaction, ed. I. Slaus (North-Holland, Amsterdam, 1972) p. 475
- 59) H.C. Catron *et al.*, Phys. Rev. **123** (1961) 218
- 60) A. Horsley, Nuc. Data **A4** (1968) 321
- 61) V. Flaminio, W.G. Moorhead, D.R.O. Morrison and N. Rivoire, Compilation of cross sections III: p and \bar{p} induced reactions, report CERN-HERA 84-01 (1984)
- 62) T.P. Clements and L. Winsberg, Lawrence Radiation Laboratory report UCRL-9043 (1960)
- 63) J. Bystricky and F. Lehar, Nucleon-nucleon scattering data: summary tables (Fachinformationszentrum Energie Physik Mathematik, Karlsruhe, 1981)
- 64) Z. Frankel, Phys. Rev. **130** (1963) 2407
- 65) P. Danielewicz, Ph.D. Thesis, Warsaw University, 1981
- 66) H.M. Pilkuhn, Relativistic particle physics (Springer, New York, 1979)
- 67) T. Udagawa, S.-W. Hong and F. Osterfeld, Phys. Lett. **B245** (1990) 1
- 68) B.J. VerWest and R.A. Arndt, Phys. Rev. **C25** (1982) 1979
- 69) E. Oset, H. Toki and W. Weise, Phys. Reports **83** (1982) 281
- 70) J.H. Koch, E.J. Moniz and N. Ohtsuka, Ann. of Phys. **154** (1984) 99
- 71) Particle Data Group, Phys. Lett. **B239** (1990) 1
- 72) P. Danielewicz and G.F. Bertsch, in preparation
- 73) P.J. Siemens, M. Soyeur, G.D. White, L.J. Lantto and K.T.R. Davies, Phys. Rev. **C40** (1989) 2641
- 74) S.-J. Wang, B.-A. Li, W. Bauer and J. Randrup, report MSUCL-752, accepted for Annals of Physics
- 75) S. Mrówczyński, Ann. of Phys. **169** (1986) 48
- 76) G. Baym and S.A. Chin, Nucl. Phys. **A262** (1976) 527
- 77) K.G.R. Doss, H.-Å. Gustafsson, H.H. Gutbrod, B. Kolb, H. Löhner, B. Ludewigt, A.M. Poskanzer, T. Renner, H. Riedesel, H.G. Ritter, A. Warwick and H. Wieman, Phys. Rev. **C32** (1985) 116
- 78) K.G.R. Doss, H.-Å. Gustafsson, H.H. Gutbrod, D. Hahn, K.-H. Kampert, B. Kolb, H. Löhner, A.M. Poskanzer, H.G. Ritter, H.R. Schmidt and H. Stöcker, Phys. Rev. **C37** (1988) 163
- 79) P.J. Siemens and J.I. Kapusta, Phys. Rev. Lett. **43** (1979) 1486
- 80) G.F. Bertsch, Nucl. Phys. **A400** (1983) 221c
- 81) J. Kapusta, Phys. Rev. **C29** (1984) 1735
- 82) K.K. Gudima, V.D. Toneev, G. Röpke and H. Schulz, Phys. Rev. **C32** (1985);
H. Schulz, G. Röpke, K.K. Gudima and V.D. Toneev, Phys. Rev. **C34** (1986) 1294
- 83) L.P. Csernai, J.I. Kapusta, G. Fai, D. Hahn, J. Randrup and H. Stöcker, Phys. Rev. **C35** (1987) 1297
- 84) P.R. Subramanian, L.P. Csernai, H. Stöcker, J.A. Maruhn, W. Greiner and H. Kruse, J. of Phys. **G7** (1981) L241;
H. Stöcker, G. Buchwald, G. Graebner, P. Subramanian, J.A. Maruhn, W. Greiner, B.V. Jacak and G.D. Westfall, Nucl. Phys. **A400** (1983) 63c
- 85) P. Danielewicz and P. Schuck, report MSUCL-775 (1991)
- 86) W.H. Press *et al.*, Numerical recipes (Cambridge Univ. Press, Cambridge, 1986)